LETTER

doi:10.1038/nature23286

Derivation of ground-state female ES cells maintaining gamete-derived DNA methylation

Masaki Yagi[1], Satoshi Kishigami[2], Akito Tanaka[1], Katsunori Semi[1], Eiji Mizutani[2,3], Sayaka Wakayama[2,3], Teruhiko Wakayama[2,3], Takuya Yamamoto[1,4] & Yasuhiro Yamada[1]

Inhibitors of Mek1/2 and Gsk3β, known as 2i, enhance the derivation of embryonic stem (ES) cells and promote ground-state pluripotency in rodents[1,2]. Here we show that the derivation of female mouse ES cells in the presence of 2i and leukaemia inhibitory factor (2i/L ES cells) results in a widespread loss of DNA methylation, including a massive erasure of genomic imprints. Despite this global loss of DNA methylation, early-passage 2i/L ES cells efficiently differentiate into somatic cells, and this process requires genome-wide *de novo* DNA methylation. However, the majority of imprinting control regions (ICRs) remain unmethylated in 2i/L-ES-cell-derived differentiated cells. Consistently, 2i/L ES cells exhibit impaired autonomous embryonic and placental development by tetraploid embryo complementation or nuclear transplantation. We identified the derivation conditions of female ES cells that display 2i/L-ES-cell-like transcriptional signatures while preserving gamete-derived DNA methylation and autonomous developmental potential. Upon prolonged culture, however, female ES cells exhibited ICR demethylation regardless of culture conditions. Our results provide insights into the derivation of female ES cells reminiscent of the inner cell mass of preimplantation embryos.

Mouse ES cells derived from the inner cell mass (ICM) of preimplantation embryos exhibit pluripotency that is shared with ICM cells *in vivo*. Culture media supplemented with fetal bovine serum (FBS) have been used for the derivation and maintenance of ES cells. However, ES cells in serum display heterogeneity and fluctuate between naive ICM-like state and primed epiblast-like state[3]. Notably, the inhibition of Mek1/2 and Gsk3β (2i) maintains ES cells in a more homogenous naive ground state[4]. Consistently, 2i-treated ES cells show global transcriptional profiles reminiscent of ICM cells with reduced DNA methylation[5–9]. Moreover, 2i treatment promotes the derivation of ES cells in rodents and possibly other mammals *in vitro*[10–12]. Nevertheless, the quality and stability of 2i-established ES cells still remains to be fully elucidated.

To explore the epigenetic and functional properties of 2i-established ES cells, we derived mouse ES cells from F_1 (129X1/SvJ and MSM/Ms) blastocysts in which their parental alleles are distinguishable by a large number of single nucleotide polymorphisms (SNPs)[13]. The genetically matched ES cells were established under one of two culture conditions, serum plus leukaemia inhibitory factor (LIF) (S/L) or 2i plus LIF (2i/L), and early passaged ES cells (passage number 3, p3) were used for further molecular analyses (Fig. 1a). We first carried out quantitative analysis of genome-wide DNA methylation of S/L and 2i/L ES cells (Extended Data Fig. 1). Consistent with previous studies[5,6], 2i treatment induced a significant and widespread reduction of DNA methylation in ES cells that was more prominent in female ES cells (Fig. 1b and Extended Data Fig. 2a, b)[6,7,14,15]. We confirmed that early-passage female 2i/L ES cell lines (p3) maintain normal karyotypic patterns (Extended Data Fig. 2c).

In contrast to previous reports[5–8], DNA methylation levels at ICRs and intracisternal A particles (IAPs) were markedly decreased in 2i/L ES cells (p3; Fig. 1c, d). The reduction of global and ICR methylation levels was detected even at p1 (Extended Data Fig. 2d). We next performed allelic analysis of the DNA methylation, which includes imprints (Fig. 1e and Extended Data Fig. 2e, f). Notably, DNA methylation at ICRs had already been eroded in male 2i/L ES cells and almost erased in female 2i/L ES cells at p3 (Fig. 1e and Extended Data Fig. 3a–c). Consistent with the reduction of ICR methylation, both male and female 2i/L ES cells showed biallelic expression of imprinted genes (Fig. 1f and Extended Data Fig. 3d). Collectively, we conclude that 2i/L ES cells exhibit defects in genomic imprints.

Because female 2i/L ES cells lack most DNA methylation, we next investigated the dynamics of DNA methylation in female 2i/L ES cells after exposure to S/L for 28 days (2i/L-S/L ES cells; Fig. 2a). 2i/L-S/L ES cells (p14) exhibited a substantial increase in global DNA methylation (Fig. 2b, c). Despite genome-wide erasure of DNA methylation, 2i/L ES cells formed teratomas and efficiently contributed to a wide variety of cells in E14.5 embryos (Fig. 2d and Extended Data Fig. 3e, f). We then obtained 2i/L-ES cell-derived mouse embryonic fibroblasts (2i/L-MEFs) (p5; Fig. 2a) and analysed global DNA methylation patterns. We observed a further gain of *de novo* DNA methylation in 2i/L-MEFs (Extended Data Fig. 3g), suggesting that female 2i/L ES cells efficiently contribute to chimaeric embryos as they undergo *de novo* methylation during development. As DNA methylation is essential for normal development[16], 2i/L ES cells with *Dnmt1* knocked out or a double knockout of both *Dnmt3a* and *Dnmt3b* ceased to grow upon the induction of differentiation and did not contribute to E14.5 embryos at all (Extended Data Fig. 4 and Supplementary Fig. 1), demonstrating that *de novo* and maintenance methylation are essential for the differentiation of 2i/L ES cells.

Importantly, *de novo* methylation was not observed at ICRs in either 2i/L-S/L ES cells or 2i/L-MEFs (Fig. 2e and Extended Data Fig. 5a, b), which is consistent with the previous finding that ES cells and somatic cells lack the ability to restore imprints[17–19]. We also detected biallelic expression of imprinted genes in both 2i/L-S/L ES cells and 2i/L-MEFs (Fig. 2f and Extended Data Fig. 5c). Apart from ICRs, most oocyte/sperm differentially methylated regions (DMRs) gained *de novo* methylation in 2i/L-S/L ES cells and 2i/L-MEFs (Extended Data Fig. 5d). Notably, secondary DMRs often gained aberrant *de novo* methylation in 2i/L-MEFs, demonstrating that despite efficient contribution to embryos, 2i/L-MEFs harbour abnormal DNA methylation patterns in conjunction with the loss of ICR methylation (Extended Data Fig. 5e, f).

As reported previously[2], we found that 2i/L ES cells are consistently able to form chimaeric embryos that exhibit a high contribution of ES-cell-derived cells (Extended Data Fig. 6a). Considering that aberrant imprinting is often linked to abnormal development and various diseases[17,20–22], we next tested whether 2i/L ES cell nuclei have the

[1]Department of Life Science Frontiers, Center for iPS Cell Research and Application (CiRA), Kyoto University, Kyoto 606-8507, Japan. [2]Faculty of Life and Environmental Sciences, University of Yamanashi, Kofu, Yamanashi 400-8510, Japan. [3]Advanced Biotechnology Center, University of Yamanashi, Kofu, Yamanashi 400-8510, Japan. [4]AMED-CREST, AMED 1-7-1 Otemachi, Chiyodaku, Tokyo 100-0004, Japan.

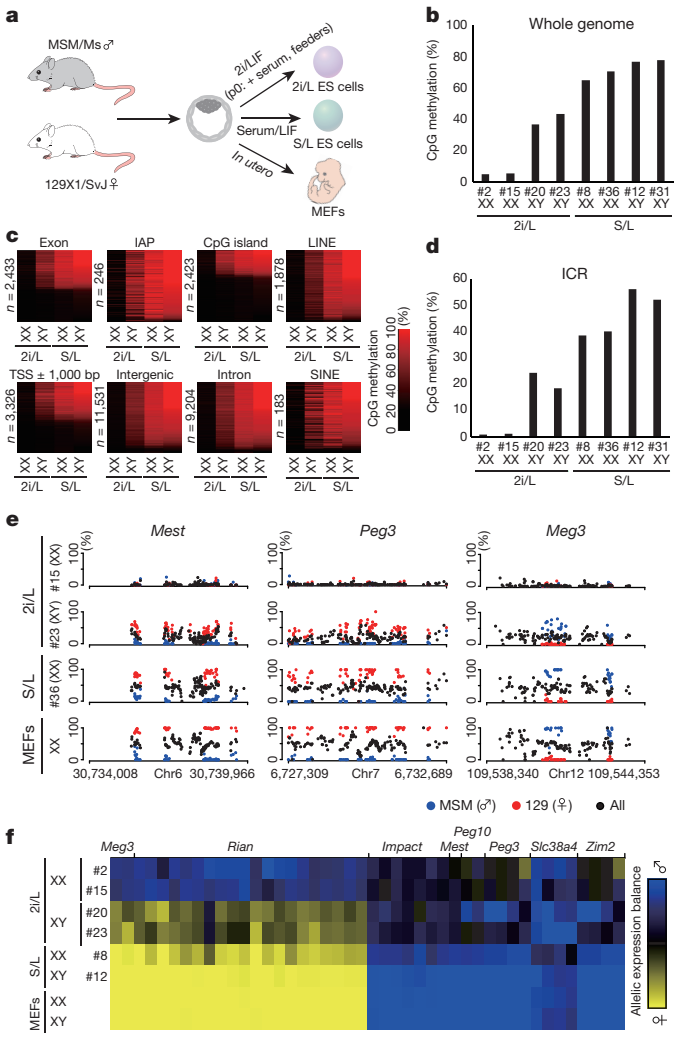

Figure 1 | Global reduction of DNA methylation and loss of imprints in 2i/L ES cells. a, Derivation of ES cells in 2i and serum from F_1 blastocyst (129/MSM). For 2i/L ES cell derivation, 2i medium containing 15% FBS and feeders were used at p0 for better attachment of blastocysts. Serum-free 2i medium without feeders was used after p1. **b**, Global CpG methylation percentage measured by whole-genome bisulfite sequencing (WGBS). The number indicates each ES cell clone. Two independent XX and XY clones were analysed for 2i/L and S/L ES cells. **c**, Heat map for CpG methylation at genomic elements in 2i/L ES cells (#15, XX and #23, XY) and S/L ES cells (#36, XX and #31, XY). DNA methylation percentages of individual CpG sites are shown in the heat map. Each *n* indicates the number of examined CpG sites. TSS, transcription start site. **d**, ICR methylation percentage measured by WGBS. Two independent XX and XY clones were analysed for 2i/L and S/L ES cells. **e**, CpG methylation at ICRs of 2i/L ES cells (#15, XX and #23, XY), S/L ES cells (#36, XX) and MEFs (#4, XX). Each black dot represents a methylation percentage for each CpG site. Red and blue dots indicate methylation levels at maternal allele and paternal allele, respectively. **f**, Allelic expression analysis of 2i/L ES cells, S/L ES cells and MEFs.

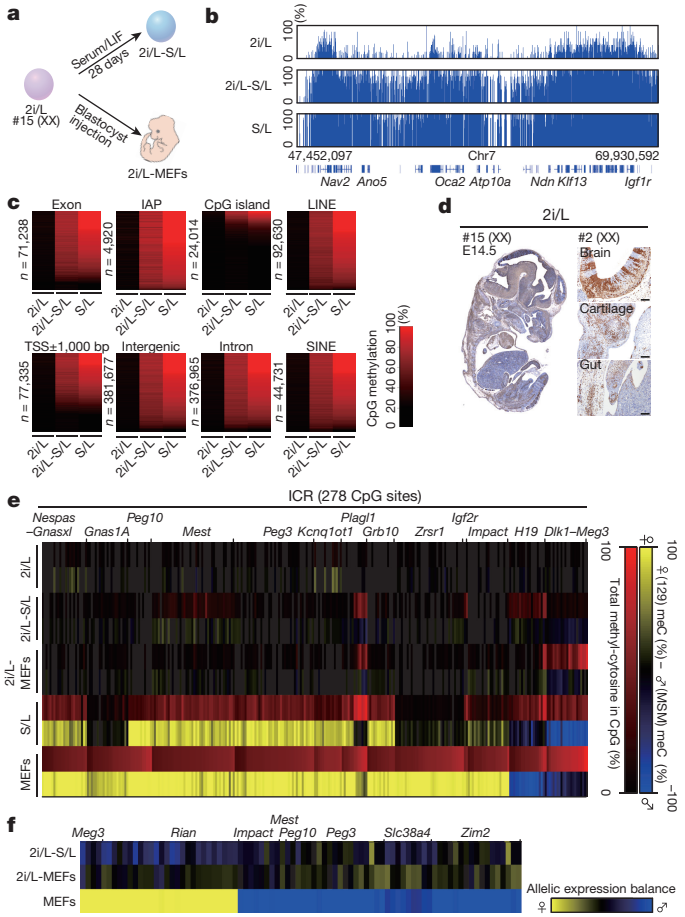

Figure 2 | Dynamics of DNA methylation of 2i/L ES cells upon differentiation. a, Derivation of 2i/L-S/L ES cells and 2i/L-MEFs. For the establishment of 2i/L-S/L ES cells, 2i/L ES cells were cultivated in S/L medium for 28 days. 2i/L-MEFs were obtained by 2*n* injection of GFP-labelled 2i/L ES cells. **b**, Global methylation level by WGBS. Each bar indicates a CG site, and the height of the bar represents methylation percentage. Location of RefSeq genes and gene symbols for representative genes are indicated below. **c**, Heat map of CpG methylation at genomic elements. Each *n* indicates the number of examined CpG sites. **d**, Efficient contribution of 2i/L ES cells to E14.5 embryos (chimaeric embryos $n = 5$ for #15 and $n = 8$ for #2). Brown colour indicates GFP staining. Scale bars, 100 μm. **e**, Heat map for ICR methylation in 2i/L ES cells (#15, XX), 2i/L-S/L ES cells (#15, XX), 2i/L-MEFs (#15, XX), S/L ES cells (#36, XX) and control MEFs (#4, XX). **f**, Allelic expression analysis of 2i/L-S/L ES cells and 2i/L-MEFs. Data for MEFs are the same as Fig. 1f.

autonomous potential for full-term development using somatic cell nuclear transfer (p4–p5; Fig. 3a)[23]. 2i/L and S/L ES cell nuclei, both of which have normal karyotypes, were competent for early development into 2-cell-stage embryos at high percentages (Extended Data Fig. 6b). However, cloned embryos from 2i/L ES cell nuclei often exhibited growth retardation around embryonic day 10.5 (Extended Data Fig. 6c), and cloned pups were exclusively obtained from S/L ES cell nuclei (Fig. 3b and Extended Data Fig. 6d). Similarly, the placentae from 2i/L-ES-cell-cloned embryos (E10.5) often exhibited hypoplasia of the labyrinth layer and focal necrosis (Fig. 3c and Extended Data Fig. 6e). Notably, the 2i/L-ES-cell-cloned placentae often showed impaired cellular adhesion with reduced expression of membranous E-cadherin (Extended Data Fig. 6f), which phenocopies trophectoderm cells lacking maternal DNA methylation[24]. To confirm the developmental defects of 2i/L ES cells with an independent assay, we next performed tetraploid embryo complementation using 2i/L and S/L ES cells (p5–p7; Fig. 3a)[25]. As shown in Fig. 3d and Extended Data Fig. 6g, h, full term all-ES-cell mice were only obtained from S/L ES cells. Collectively, these results indicate that female 2i/L ES cells lacking heritable DNA methylation harbour impaired autonomous developmental potential.

To gain molecular insights into the developmental defects of 2i/L ES cell nuclei, we next employed the *Cdx2*-mediated trophectoderm differentiation protocol on ES cells[26]. After *Cdx2* overexpression, the formation of trophoblast stem cell (TSC)-like colonies was severely impaired in 2i/L ES cells (Extended Data Fig. 7a, b). Of note, *Scml2*, the suppression of which by maternal DNA methylation plays a role in proper placental development[24], was derepressed in 2i/L ES cells (Extended Data Fig. 7c–f). Finally, we found that the impaired TSC-like colony formation in *Cdx2*-induced 2i/L ES cells is

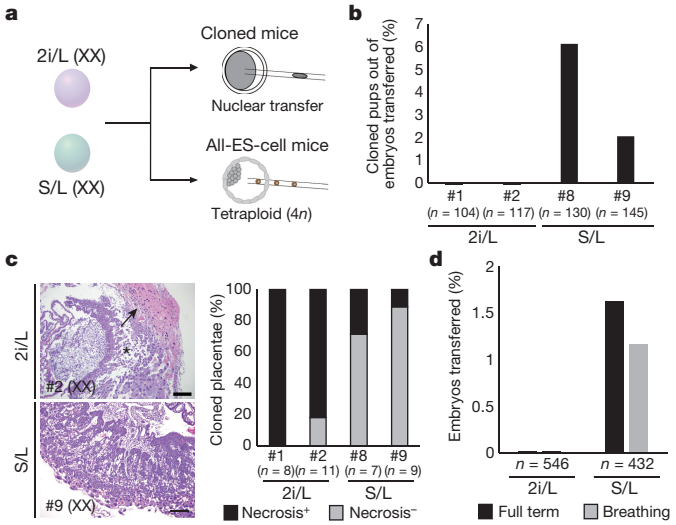

Figure 3 | Impaired full-term developmental potential of 2i/L ES cells. **a**, Strategy for assessing developmental potential of 2i/L ES cells. **b**, Graph shows percentage of embryos transferred that gave rise to cloned pups. *n* indicates the number of embryos transferred. **c**, Histological analysis of the cloned placentae (E10.5). Scale bars, 500 μm. Asterisk indicates hypoplasia of labyrinth layer and impaired cell adhesion. Arrow denotes focal necrosis. Incidence of the placentae with focal necrosis is shown (*n* indicates the number of cloned placentae examined). **d**, Graph shows percentage of embryos transferred that gave rise to all-ES-cell pups (2i/L #1, #2 and S/L #8). *n* indicates the number of embryos transferred.

partially rescued by genetic ablation of *Scml2* (S/L, $51.8 \pm 9.4\,cm^{-2}$; 2i/L, $0.6 \pm 0.5\,cm^{-2}$; *Scml2*-knockout 2i/L, $6.4 \pm 1.2\,cm^{-2}$; Extended Data Fig. 7g, h). Collectively, these results suggest that the derepression of *Scml2* is involved in abnormal placental development in 2i/L-ES-cell-cloned embryos, which is similarly observed in embryos deficient in maternal DNA methylation[24]. We also compared DNA methylation and gene expressions of 2i/L-MEFs derived from all-ES-cell embryos (4*n* 2i/L-MEFs; E14.5) with those from chimaeric embryos (2*n* 2i/L-MEFs; E14.5). Although no detectable difference in DNA methylations was observed between 4*n* 2i/L-MEFs and 2*n* 2i/L-MEFs (Extended Data Fig. 7i), many imprinted genes, as well as other genes, were aberrantly expressed in 4*n* 2i/L-MEFs, whereas the aberration was less obvious in 2*n* 2i/L-MEFs, presumably owing to non-cell-autonomous effects (Extended Data Fig. 7j). Together, our results show that loss of gamete-derived methylation is associated with impaired autonomous development of 2i/L ES cells.

Considering the critical role of heritable DNA methylation in embryogenesis, we next tried to establish ground-state ES cells that retain gamete-derived DNA methylation. Previous studies suggested a possible link between the inhibition of MAPK signalling in female ES cells and the reduction of global DNA methylation, including ICRs[15,27,28]. Thus, we established ES cells under either a low concentration of Mek1/2 inhibitor PD0325901 (referred to as PD) (t2i/L; 0.2 μM PD, 3 μM Gsk3β inhibitor CHIR99021 (referred to as CHIR), and LIF) or alternative 2i in which the Mek1/2 inhibitor is substituted with a Src inhibitor CGP77675 (referred to as CGP) (a2i/L; 1.5 μM CGP, 3 μM CHIR, and LIF) (Extended Data Fig. 8a, b)[29]. As expected, t2i/L and a2i/L attenuated the repression of Mek target genes[27] in both male and female ES cells (p3; Extended Data Fig. 8c–e, Supplementary Fig. 1). Of note, both t2i/L and a2i/L enhanced the derivation of ES cells from F_1 (129X1/SvJ and C57BL/6) blastocysts to a similar extent as 2i/L (Fig. 4a). Moreover, they enabled ES cell derivation from non-permissive mouse strains (BALB/c, C3H and DBA2; Fig. 4b). Consistent with the notion that t2i/L and a2i/L promote ground-state pluripotency, the gene expression patterns of t2i/L and a2i/L ES cells were reminiscent of conventional 2i/L ES cells and were distinguishable from S/L ES cells (p3; Fig. 4c and Extended Data Fig. 8f). Most notably, t2i/L and a2i/L ES cells preserved ICR methylation while exhibiting a reduction of genome-wide DNA methylation (p3; Fig. 4d and Extended Data Fig. 8g, h). In accordance with the remaining methylation at ICRs, t2i/L and a2i/L ES cells tended to retain monoallelic expression of imprinted genes (p3: Extended Data Fig. 8i). Finally, we tested the autonomous developmental potential of early-passage female t2i/L and a2i/L ES cells by tetraploid embryo complementation. In sharp contrast to female 2i/L ES cells, female a2i/L ES cells efficiently gave rise to all-ES-cell mice (p4; Fig. 4e and Extended Data Fig. 8j, k). Similarly, female t2i/L ES cells were able to give rise to all-ES-cell mice, albeit at lower efficiency.

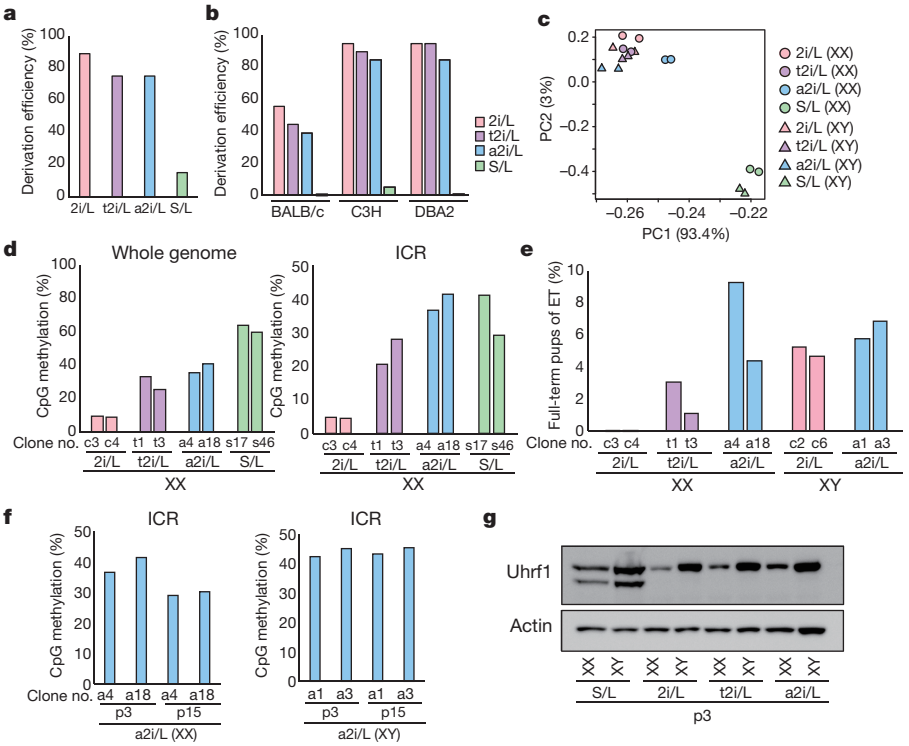

Figure 4 | Derivation of ground-state ES cells maintaining ICR methylation. **a**, Derivation efficiency of ES cells (129/B6) under various culture conditions. The number of blastocysts used for 2i/L, t2i/L, a2i/L and S/L derivation is 18, 20, 20 and 20, respectively. **b**, Derivation efficiency of ES cells from refractory mouse strains. The number of blastocysts used for ES cell derivation in BALB/c, C3H and DBA2 is 18, 20 and 20, respectively. **c**, Principal component analysis (PCA) indicated that t2i/L ES cells and a2i/L ES cells exhibit similar expression signatures with 2i/L ES cells (independent ES cell clones; $n = 2$ for each condition and sex). All expressed genes, including X-linked genes, were used for this analysis. **d**, DNA methylation percentage measured by WGBS in various ES cell lines ($n = 2$ for each condition). **e**, Percentage of 4*n* embryos transferred (ET) that developed full-term pups. **f**, ICR methylation of female and male a2i/L ES cells after prolonged culture. Methylation data of female and male a2i/L ES cells at p3 are the same as in **d** and Extended Data Fig. 8g, respectively. **g**, Western blot analysis of Uhrf1 in ES cells cultured in various conditions.

These data suggest that modified culture conditions, particularly a2i/L conditions, preserve the epigenetic stability of genomic imprints and developmental potential of early-passage female ES cells.

However, after prolonged culture, female a2i/L ES cells, as well as female t2i/L ES cells, at p15 showed a reduction of ICR methylation, which was similarly observed in S/L ES cells at p15, while male a2i/L ES cells at p15 retained ICR methylation (Fig. 4f and Extended Data Fig. 9a, b). In addition, reduction of Uhrf1 protein, as well as Dnmt3a and Dnmt3b proteins[14,15], was observed in female a2i/L ES cells (p3; Fig. 4g, Extended Data Fig. 9c, d and Supplementary Fig. 1), suggesting that impaired maintenance of DNA methylation leads to ICR demethylation in female a2i/L ES cells. As reported recently[15], neither XO ES cells nor XX MEFs exhibit reduced levels of Uhrf1, indicating that two active X chromosomes cause the reduced expression of Uhrf1 (Extended Data Fig. 9d–g and Supplementary Fig. 1).

In contrast to the decreased ICR methylation, we found that genome-wide DNA methylation was increased in female a2i/L ES cells at p15 (Extended Data Fig. 10a). Similarly, female 2i/L ES cells at p15 showed increased global DNA methylation compared with early-passage 2i/L ES cell lines (p3; Extended Data Fig. 10a), which indicates that female 2i/L and a2i/L ES cells gained *de novo* methylation during prolonged culture. Consistently, the protein levels of Uhrf1 and Dnmt3b were higher in p15 female 2i/L and a2i/L ES cells than at p3 (Extended Data Fig. 10b, c and Supplementary Fig. 1). Notably, we found that female ES cells at p15 display a loss of X chromosome to varying degrees (Extended Data Fig. 10d, e), suggesting that the loss of two active X chromosomes causes, at least in part, increased Uhrf1 and Dnmt3b at p15.

These results, taken together, show that the derivation of ES cells under 2i/L results in a widespread reduction of DNA methylation, including gamete-derived methylation. These ES cells exhibit impairment in embryonic and placental development, which reveals the limitations of 2i/L-established ES cells for the quality of pluripotent stem cells. Our findings are important for the understanding of human naive-like pluripotent stem cells with regards to therapeutic applications and disease modelling, since imprints and oocyte-derived methylation memory are often lost in these cells[19,30]. We also show that early-passage female a2i/L ES cells and t2i/L ES cells retain gamete-derived DNA methylation and autonomous developmental potential. We propose that these ES cells may serve as an alternative cell-culture platform for dissecting the biology of early embryogenesis.

Online Content Methods, along with any additional Extended Data display items and Source Data, are available in the online version of the paper; references unique to these sections appear only in the online paper.

Received 13 June 2016; accepted 19 June 2017.
Published online 26 July 2017.

1. Nichols, J. & Smith, A. Naive and primed pluripotent states. *Cell Stem Cell* **4,** 487–492 (2009).
2. Hackett, J. A. & Surani, M. A. Regulatory principles of pluripotency: from the ground state up. *Cell Stem Cell* **15,** 416–430 (2014).
3. Smith, Z. D. *et al.* A unique regulatory phase of DNA methylation in the early mammalian embryo. *Nature* **484,** 339–344 (2012).
4. Ying, Q. L. *et al.* The ground state of embryonic stem cell self-renewal. *Nature* **453,** 519–523 (2008).
5. Ficz, G. *et al.* FGF signaling inhibition in ES cells drives rapid genome-wide demethylation to the epigenetic ground state of pluripotency. *Cell Stem Cell* **13,** 351–359 (2013).
6. Habibi, E. *et al.* Whole-genome bisulfite sequencing of two distinct interconvertible DNA methylomes of mouse embryonic stem cells. *Cell Stem Cell* **13,** 360–369 (2013).
7. Hackett, J. A. *et al.* Synergistic mechanisms of DNA demethylation during transition to ground-state pluripotency. *Stem Cell Reports* **1,** 518–531 (2013).
8. Leitch, H. G. *et al.* Naive pluripotency is associated with global DNA hypomethylation. *Nat. Struct. Mol. Biol.* **20,** 311–316 (2013).
9. Marks, H. *et al.* The transcriptional and epigenomic foundations of ground state pluripotency. *Cell* **149,** 590–604 (2012).
10. Buehr, M. *et al.* Capture of authentic embryonic stem cells from rat blastocysts. *Cell* **135,** 1287–1298 (2008).
11. Czechanski, A. *et al.* Derivation and characterization of mouse embryonic stem cells from permissive and nonpermissive strains. *Nat. Protocols* **9,** 559–574 (2014).
12. Guo, G. *et al.* Naive pluripotent stem cells derived directly from isolated cells of the human inner cell mass. *Stem Cell Reports* **6,** 437–446 (2016).
13. Takada, T. *et al.* The ancestor of extant Japanese fancy mice contributed to the mosaic genomes of classical inbred strains. *Genome Res.* **23,** 1329–1338 (2013).
14. Zvetkova, I. *et al.* Global hypomethylation of the genome in XX embryonic stem cells. *Nat. Genet.* **37,** 1274–1279 (2005).
15. Choi, J. *et al.* DUSP9 modulates DNA hypomethylation in female mouse pluripotent stem cells. *Cell Stem Cell* **20,** 706–719.e7 (2017).
16. Li, E., Bestor, T. H. & Jaenisch, R. Targeted mutation of the DNA methyltransferase gene results in embryonic lethality. *Cell* **69,** 915–926 (1992).
17. Holm, T. M. *et al.* Global loss of imprinting leads to widespread tumorigenesis in adult mice. *Cancer Cell* **8,** 275–285 (2005).
18. Tucker, K. L. *et al.* Germ-line passage is required for establishment of methylation and expression patterns of imprinted but not of nonimprinted genes. *Genes Dev.* **10,** 1008–1020 (1996).
19. Theunissen, T. W. *et al.* Molecular criteria for defining the naive human pluripotent state. *Cell Stem Cell* **19,** 502–515 (2016).
20. Kato, Y. *et al.* Developmental potential of mouse primordial germ cells. *Development* **126,** 1823–1832 (1999).
21. Ohnishi, K. *et al.* Premature termination of reprogramming *in vivo* leads to cancer development through altered epigenetic regulation. *Cell* **156,** 663–677 (2014).
22. Stadtfeld, M. *et al.* Aberrant silencing of imprinted genes on chromosome 12qF1 in mouse induced pluripotent stem cells. *Nature* **465,** 175–181 (2010).
23. Wakayama, T., Perry, A. C., Zuccotti, M., Johnson, K. R. & Yanagimachi, R. Full-term development of mice from enucleated oocytes injected with cumulus cell nuclei. *Nature* **394,** 369–374 (1998).
24. Branco, M. R. *et al.* Maternal DNA methylation regulates early trophoblast development. *Dev. Cell* **36,** 152–163 (2016).
25. Nagy, A., Rossant, J., Nagy, R., Abramow-Newerly, W. & Roder, J. C. Derivation of completely cell culture-derived mice from early-passage embryonic stem cells. *Proc. Natl Acad. Sci. USA* **90,** 8424–8428 (1993).
26. Niwa, H. *et al.* Interaction between Oct3/4 and Cdx2 determines trophectoderm differentiation. *Cell* **123,** 917–929 (2005).
27. Schulz, E. G. *et al.* The two active X chromosomes in female ES cells block exit from the pluripotent state by modulating the ES cell signaling network. *Cell Stem Cell* **14,** 203–216 (2014).
28. Shirane, K. *et al.* Global landscape and regulatory principles of DNA methylation reprogramming for germ cell specification by mouse pluripotent stem cells. *Dev. Cell* **39,** 87–103 (2016).
29. Shimizu, T. *et al.* Dual inhibition of Src and GSK3 maintains mouse embryonic stem cells, whose differentiation is mechanically regulated by Src signaling. *Stem Cells* **30,** 1394–1404 (2012).
30. Pastor, W. A. *et al.* Naive human pluripotent cells feature a methylation landscape devoid of blastocyst or germline memory. *Cell Stem Cell* **18,** 323–329 (2016).

Supplementary Information is available in the online version of the paper.

Acknowledgements We are grateful to T. Shiroishi, M. Saitou and S. Yokobayashi for helpful suggestions, K. Woltjen for providing *piggyBac* vectors, P. Karagiannis for critical reading of this manuscript, and T. Ukai, M. Kabata, S. Sakurai, D. Seki and T. Sato for technical assistance. Y.Y. was supported in part by P-CREATE, SICORP, Japan Agency for Medical Research and Development (AMED); JSPS KAKENHI 15H04721; the Princess Takamatsu Cancer Research Fund; the Takeda Science Foundation; and the Naito Foundation. Y.Y. and T.Y. were supported by Core Center for iPS Cell Research, Research Center Network for Realization of Regenerative Medicine, AMED. T.Y. was supported by AMED-CREST; JSPS KAKENHI 15H01352; and iPS Cell Research Fund. M.Y. was supported by JSPS KAKENHI 15J05792.

Author Contributions M.Y. and Y.Y. designed and conceived the study and wrote the manuscript. M.Y. generated cell lines, performed experiments, analysed microarray data and generated WGBS and methyl-seq libraries. S.K., E.M., S.W. and T.W. performed nuclear transfer. K.S. provided technical instructions. A.T., S.K., S.W. and T.W. performed 2*n* and 4*n* blastocyst injections. T.Y. analysed all the WGBS, methyl-seq and RNA-seq data.

Author Information Reprints and permissions information is available at www.nature.com/reprints. The authors declare no competing financial interests. Readers are welcome to comment on the online version of the paper. Publisher's note: Springer Nature remains neutral with regard to jurisdictional claims in published maps and institutional affiliations. Correspondence and requests for materials should be addressed to Y.Y. (y-yamada@cira.kyoto-u.ac.jp) and T.Y. (takuya@cira.kyoto-u.ac.jp).

Reviewer Information *Nature* thanks T. Zwaka and the other anonymous reviewer(s) for their contribution to the peer review of this work.

METHODS

Data reporting. No statistical methods were used to predetermine sample size. The experiments were not randomized and the investigators were not blinded to allocation during experiments and outcome assessment.

Establishment and culture of MEFs and ES cells. Zygotes with an F_1 genetic background (129X1/SvJ and MSM/Ms[13,31] or 129X1/SvJ and C57BL/6) were obtained by *in vitro* fertilization (IVF). Cells were maintained at 37 °C with 5% CO_2. MEFs were isolated from E14.5 embryos and were cultured in DMEM (Nacalai Tesque) with 2 mM L-glutamine (Nacalai Tesque), 100 × non-essential amino acids (NEAA) (Nacalai Tesque), 100 U ml^{-1} penicillin, 100 μg ml^{-1} streptomycin (P/S) (Nacalai Tesque) and 10% fetal bovine serum (FBS) (GIBCO). S/L cells were established and maintained on feeders (mitomycin C-treated MEFs) in knockout DMEM (GIBCO) with 2 mM L-glutamine, 100 × NEAA, P/S, 15% FBS, 0.11 mM β-mercaptoethanol (GIBCO) and 1,000 U ml^{-1} human recombinant leukaemia inhibitory factor (LIF) (Wako). For the establishment of S/L ES cells, a blastocyst was placed on feeders in 24-well plates (passage number 0: p0). After the expansion of ICM, the cells were passaged into 24-well plates (p1), followed by a second passage into 6-well plates (p2) and then a third passage into 6-cm dishes (p3). For the derivation of 2i/L ES cells, t2i/L ES cells and a2i/L ES cells, blastocyst was placed on feeders in 24-well plates with knockout DMEM containing 2 mM L-glutamine, 100 × NEAA, P/S, 15% FBS, 0.11 mM β-mercaptoethanol and 1,000 U ml^{-1} LIF, which was supplemented with 1 μM PD0325901 (STEMGENT) and 3 μM CHIR99021 (STEMGENT) for 2i/L, 0.2 μM PD0325901 and 3 μM CHIR99021 for t2i/L, and 1.5 μM CGP77675 (Sigma) and 3 μM CHIR99021 for a2i/L (p0). After passage into 24-well plates (p1), the cells were maintained without feeders in DMEM/F12 (GIBCO) and Neurobasal (GIBCO) supplemented with B27 (GIBCO) and N2 cell-supplements (GIBCO), P/S, 2 mM Glutamax (GIBCO), and 1,000 U ml^{-1} LIF, which was supplemented with 1 μM PD0325901 and 3 μM CHIR99021 for 2i/L, 0.2 μM PD0325901 and 3 μM CHIR99021 for t2i/L, and 1.5 μM CGP77675 and 3 μM CHIR99021 for a2i/L. Cells were passaged into 6-well plates (p2) and expanded into 6-cm dishes (p3). ES cell lines at p3 were stocked and used for further experiments. To obtain 2i/L-S/L ES cells, 2i/L ES cells were cultured on feeders in S/L for 28 days. For the sample preparation of S/L ES cells and 2i/L-S/L ES cells, SSEA1-positive cells were sorted by fluorescence-activated cell sorting (FACS) (Aria II, BD) to remove feeders. Alexa Fluor 647-conjugated anti-SSEA1 (Santa Cruz, sc-21702 AF647) was used for the sorting.

Animals. All experiments using animals were performed under the ethical guidelines of Kyoto University and University of Yamanashi. MSM/Ms were obtained from RIKEN Bio Resource Center[13,31]. C57BL/6, 129X1/SvJ, B6D2F1, BALB/c, C3H/He, DBA/2, ICR mice, pseudo-pregnant ICR mice and BALB/cSlc-nu/nu mice were purchased from SLC. Noon of the day when the plug was observed was designated as embryonic day (E) 0.5.

Cell line availability. The *Dnmt* triple-knockout ES cell line was obtained from RIKEN Bio Resource Center (RBRC-AES0146)[32]. Other cell lines were derived in our laboratory and tested for mycoplasma contamination.

Gender determination. The gender of cell lines was determined by PCR using primers for *Sry* and *Uty*, located on the Y chromosome. The primers used were: *Sry* forward: CGTGGTGAGAGGCACAAGTT; *Sry* reverse: AGGCAACTG CAGGCTGTAAA; *Uty* forward: GAGTTCTTCTTGCGTTCACCATCTG; and *Uty* reverse: CTATCTAATCCACAAAGCGCCTTCTTC.

Karyotyping. Female 2i/L ES cells (#1 and #2; XX, p3, 129/MSM), female S/L ES cells (#8 and #9; XX, p3, 129/MSM) and S/L XO ES cells (#s100; p3, 129/C57BL6) were used for the karyotype analysis. Cells were treated with 0.025, 0.013 and 0.007 μg ml^{-1} demecolcine (Sigma) for 1 h at 37 °C with 5% CO_2. Cells were tripsinized for single cell suspension and incubated with 0.075 M KCL (Wako) for 7 min at room temperature. Then the treated cells were fixed using Carnoy fluid (acetic acid: methanol = 1:3). 20 cells were analysed by Q-band.

GFP labelling of ES cells. ES cells (p3) were labelled by *piggyBac* (PB) transposon carrying CAG-EGFP-IRES-Neo[33]. 2.5 μg of the plasmid and 2.5 μg of Transposase were transfected into ES cells using Xfect mES cell Transfection Reagent (Clontech) according to the supplier's protocol. Transfected cells were selected by 350 μg ml^{-1} G418 Disulfate Aqueous Solution (Nacalai tesque). GFP-positive colonies were picked up and established as GFP-labelled clones (p5).

DNA/RNA extraction and cDNA synthesis. DNA was extracted by PureLink Genomic DNA Mini Kit (Invitrogen) and RNA was extracted by RNAeasy plus Mini Kit (QIAGEN). DNA and RNA were quantified by Nanodrop 2000c (Thermo Scientific) and Qubit (Thermo Scientific). Reverse transcription was performed with PrimeScript II 1st strand cDNA Synthesis Kit (Takara) according to the supplier's instruction.

Quantitative RT–PCR. Quantitative PCR was performed using GoTaq qPCR Mater Mix and CXR Reference Dye according to the supplier's instruction (Promega). StepOnePlus Real-Time PCR system (Applied Biosystems) was used. Transcript levels were normalized to β-actin (*Actb*). The experiments were performed in technical triplicates. The primers used for were: *Scml2* forward: TGATTCGGTGTGTG TTGCTTC; *Scml2* reverse: AGTCGTAGACGTAACCTGGCT; *Dusp6* forward: ATAGATACGCTCAGACCCGTG; *Dusp6* reverse: ATCAGCAGAAGC CGTTCGTT; *Cldn7* forward: GGCCTGATAGCGAGCACTG; *Cldn7* reverse: GTGACGCACTCCATCCAGA; *Actb* froward: GCCAACCGTGAAAAGATGAC; and *Actb* reverse: TCCGGAGTCCATCACAATG.

Western blot. Cells were harvested in 500 μl of RIPA lysis buffer containing protease inhibitor cocktail (Nacalai Tesque), dithiothreitol (wako) and phosphatase inhibitor cocktail (Nacalai Tesque). For S/L ES cells, we removed feeders by culturing dissociated ES cells in S/L medium for 30 min and harvesting floating cell populations. Proteins were denatured with 2 × SDS at 95 °C for 5 min. A total of 30 μg denatured protein was run on 8% or 10% SDS–PAGE gel and transferred to Amersham Hybond-P PVDF Membrane (GE Healthcare) using PowerPac HC (Bio-Rad). Membranes were blocked with 4% skim milk (Nacalai Tesque) in 1 × TBS with 0.05% Tween-20 (TBST) and then incubated with primary antibodies diluted by blocking buffer (4% skim milk in TBST) overnight at 4 °C. The primary antibodies used were anti-phospho-p44/42 MAPK (CST, 20G11, 4376; dilution 1:1,000), anti- p44/42 MAPK (CST, L34F12, 4696S; dilution 1:2,000), anti-Dnmt3a (Novus Biological, NB120-13888, 64B1446; dilution 1:500; Santa Cruz, sc-20703; dilution 1:200), anti-Dnmt3b (Activemotif, 39207, 52A1018; dilution 1:125 / IMAGENEX, IMG-184A; dilution 1:500), anti-Dnmt3l (Abcam, ab3493; dilution 1:2,500), anti-Dnmt1 (COSMO BIO, 70-201EX; dilution 1:1,000), anti-Uhrf1 (Santa Cruz, sc-373750; dilution 1:100) and anti-β-actin (Santa Cruz, sc-47778; dilution 1:1,000). Blots were rinsed with TBST. Membranes were incubated with HRP-conjugated secondary antibodies for 90 min at room temperature. The secondary antibodies used were ECL anti-mouse IgG, HRP-linked whole antibody from sheep (NA931V, GE Healthcare) and ECL anti-rabbit IgG, HRP linked whole antibody from donkey (NA934V, GE Healthcare). After rinsing with TBST, Pierce ECL plus Western Blotting Substrate (Thermo Scientific) was used for visualization, and LAS4000 (GE Healthcare) was used for band detection.

Immunocytochemistry. Cells were fixed with 4% paraformaldehyde (Wako) for 15 min and were treated with PBS (Nacalai tesque) containing 0.5% Triton (Sigma) for 5 min at room temperature. Cells were then treated with PBS containing 3% FBS and 0.1% Triton and stained with anti-5mC antibody (Diagenode, Mab-006-100; dilution 1:500) overnight at 4 °C. Secondary antibodies conjugated with Alexa Fluor 488 (Invitrogen) and Hoechst 33258 (DOJINDO) were used for visualization. Immunofluorescence signals were detected by BZ-9000 (KEYENCE).

HE staining and immunohistochemistry. Samples were fixed with 4% paraformaldehyde overnight at room temperature and embedded in paraffin using Spin Tissue Processor STP120-2 (Thermo Scientific). Sections were stained with haematoxylin and eosin (HE). For immunohistochemistry, sections were treated with xylene and 100% ethanol, then washed with water followed by treatment with Histofine (Nichirei). After rinsing with PBS, sections were incubated with anti-GFP antibody (Abcam, ab183734; dilution 1:200) or anti-E-cadherin antibody (CST, 24E10, #3195S; dilution 1:400) overnight at 4 °C. Sections were then rinsed with PBS and incubated with Histofine Simple Stain Mouse MAX PO (Nichirei) containing secondary antibody for 30 min at room temperature. DAB Substrate Kit (Nichirei) was used for detection.

Microarray. Microarray analysis was performed using the Mouse Gene 1.0 ST Array (Affymetrix) in accordance with the manufacturer's instructions. Data were analysed using the GeneSpring GX software program (version 13; Agilent Technology).

Bisulfite sequencing. 200 ng of DNA was bisulfite-treated using EZ DNA Methylation-Gold Kit (ZYMO RESEARCH) according to the supplier's instruction. PCR was performed with LA Taq HS (Takara). PCR products were cloned into pCR4-TOPO vector (Invitrogen). Subcloned colonies were sequenced with a M13 reverse primer by ABI 3500xL (Applied Biosystems). The primers used were: *Peg10* DMR forward: GTAAAGTGATTGGTTTTGTATTTTTAAGTG; *Peg10* DMR reverse: TTAATTACTCTCCTACAACTTTCCAAATT; *Nespas-Gnasxl* DMR forward: GGTTTTGGGTTTTAGTTTTTGATTATTTA; and *Nespas-Gnasxl* DMR reverse: TCTTCTAAAAATCCACTAATCTCACTACC; *Snrpn* DMR forward: AATTTGTGTGATGTTTGTAATTATTTGG; and *Snrpn* DMR reverse: ATAAAATACACTTTCACTACTAAAATCCACAA.

Allelic expression analysis. A SNP (MSM/Ms: A, 129/SvJ: C) at exon1 of *Peg10* was used to distinguish parental alleles. cDNA was amplified using KOD-Plus-Neo (TOYOBO). Amplified products were cloned into pCR4-TOPO-Blunt vector (Invitrogen). Subcloned colonies were sequenced with a forward primer by ABI 3500xL. The primers were: *Peg10* forward: TGGTTCCTCCAACTGCCCG; and *Peg10* reverse: GGCGAATTCTTGGAGGCTTTCG.

Library preparation for whole-genome bisulfite sequencing (WGBS). 500 ng of DNA calculated by Qubit was fragmented by sonication (Covaris) and ligated with methylated adapters supplied by TruSeq DNA, Sample Prep Kit-v2 (Illumina). Subsequently, DNA was bisulfite-treated using EZ DNA Methylation-Gold Kit.

Final library amplification was performed using *Pfu* Turbo Cx (Agilent Technologies). Sequencing libraries were assessed by Bioanalyzer (Agilent Technologies) and quantified with KAPA Library Quantification Kits (KAPA BIOSYSTEMS). The libraries were then sequenced on HiSeq 2500 (2 × 100 bp or 2 × 101 bp paired-end reads, Illumina) or on NextSeq500 (75 bp single, Illumina).

Library preparation for target-captured bisulfite sequencing. 3 μg of DNA calculated by Qubit was fragmented by sonication. Subsequently, library preparation was performed with SureSelect^{XT} Mouse Methyl-Seq Reagent Kit (Agilent Technologies). The Methyl-Seq Kit could enrich 109 Mb of mouse genomic regions including CpG islands, Gencode promoters, DNase I hypersensitive sites and tissue-specific DMRs. DNA was bisulfite-treated using EZ DNA Methylation-Gold Kit. Sequencing libraries were assessed by Bioanalyzer and quantified with KAPA Library Quantification Kits. The libraries were then sequenced on HiSeq 2500 (2 × 100 bp or 2 × 101 bp paired-end reads, Illumina).

Library preparation for RNA sequencing. 200 ng of total RNA was prepared for library construction. High-quality RNA (RNA integrity number value ≥8) assessed by Bioanalyzer was used for library preparation. RNA-seq libraries were generated using Truseq Stranded mRNA LT sample prep kit (Illumina). Poly(A)-containing mRNA was purified by poly(T)-oligo-attached magnetic beads and the RNA was fragmented and primed for cDNA synthesis. Cleaved RNA fragments were reverse transcribed into first strand cDNA using transcriptase and random primers. Second strand cDNA was synthesized by the incorporation of dUTP and double-stranded cDNA was separated using AMPure XP beads (Beckman Coulter). A single 'A' nucleotide was added to the 3′ ends of the blunt fragments and then adapters with index were ligated to the ends of the double-stranded cDNA. Double-stranded cDNA fragments were amplified by PCR with PCR primer Cocktail. The number of PCR cycles was minimized (11–15 cycles) to avoid skewing the representation of the libraries. RNA-seq libraries were sequenced on NextSeq500 (75 bp single, Illumina).

DNA methylation data analyses. For allelic methylation analyses, the SNPs data for MSM/Ms were obtained from NIG Mouse Genome Database (MSMv4HQ, http://molossinus.lab.nig.ac.jp/msmdb/index.jsp) and MSM/Ms mouse genome was reconstructed from mm10 using the SNPs. The information about indels was not used in this study. The bases with low quality scores and the adapters in all the sequenced reads were trimmed with cutadapt 1.9.1[34]. The trimmed reads were mapped to both B6 mouse genome (mm10) and MSM/Ms mouse genome independently by Bismark software v.0.15.0[35] with bowtie2 (version 2.2.8)[36]. The reads mapped to the same chromosome and positions of both B6 and MSM/Ms genomes with high mapping quality (MAPQ ≥ 20) were used for further analyses. The B6-derived and MSM/Ms-derived sequenced reads were determined based on the MSM/Ms SNPs data. Y chromosome and M chromosome were omitted from MSM/Ms reference genome because of the lack of the SNPs data. SNPs in CpG sites were excluded and the patterns of bisulfite conversion were taken into account in the determination of parental alleles. Methylated cytosines were extracted from the reads by the Bismark methylation extractor with —ignore 10 —ignore_r2 10 —ignore_3prime 5 —ignore_3prime_r2 5. Because probe sequences of the SureSelect^{XT} were designed for original top strand, only the original bottom (OB) data were used for the analysis. For normal WGBS analysis, the trimmed reads were mapped to the mouse genome (mm10) by Bismark software v.0.15.0 with bowtie2 (version 2.2.8) and default settings, and the mapped reads with high mapping quality (MAPQ ≥ 20) were used for extraction of methylated cytosines by the Bismark methylation extractor with —ignore 10 —ignore_3prime 5 options (single-end reads) or with —ignore 10 —ignore_r2 10 —ignore_3prime 5 —ignore_3prime_r2 5 options (paired-end reads). R (v.3.1) and Integrative Genomics Viewer (IGV)[37] were used to visualize the CpG methylated status. UCSC LiftOver tools[38] (http://genome.ucsc.edu/) were used to convert the coordinates of mm9 assembly into those of mm10 assembly. In the dot plots, each dot represents the methylation percentage for a CpG site at ≥ 5× coverage. CpG sites at ≥ 5× coverage in all samples were captured by heat maps. Genomic locations for each genetic element were described previously[39–41].

RNA-seq data analyses. The sequenced reads were mapped to the mouse reference genome (mm10) using tophat 2.1.0[42] with the GENCODE version M9 annotation gtf file and the aligner Bowtie2 2.2.5[36] after trimming adaptor sequences and low-quality bases by cutadapt 1.9.1[34]. For allelic expression analysis, the trimmed reads were also mapped to MSM genomes used in the DNA methylation data analyses section, and the reads mapped to the same chromosome and positions of both B6 and MSM/Ms genomes with high mapping quality (MAPQ ≥ 20) were used for further analyses. The expression level of each gene was calculated as reads per kilobase per million mapped reads (RPKM) by cufflinks 2.2.1[43]. The target genes of Mek and Gsk3β were obtained from a previous study[27]. SNPs data for MSM/Ms were obtained as described in the DNA methylation data analyses section. Hierarchical clustering analysis and principal component analysis (PCA) were performed using R (v.3.3.1).

Array comparative genomic hybridization (aCGH). aCGH was performed using SureTag DNA Labelling Kit (Agilent Technologies). 500 ng of DNA measured by Qubit was used for sample labelling. Random primer containing DNA was incubated at 95 °C for 10 min (without restriction digestion). Labelling reactions were performed at 37 °C for 2 h with Cy3 (for reference samples) and Cy5 (for experimental samples). Labelled DNA samples were purified using reaction purification columns provided by SureTag DNA Labelling Kit. 8 × 60K aCGH Microarray was used for the hybridization. Hybridization master mix was denatured at 95 °C for 3 min exactly and then transferred to 37 °C for 30 min. The solutions were centrifuged for 1 min at 6,000*g* to collect the sample at the bottom of the tube. These mixtures were then hybridized to the Microarray at 65 °C for 24 h in a rotator rack. Microarray was washed using oligo aCGH wash buffer 1 and oligo aCGH wash buffer 2. Microarray Scanning was performed with Agilent C Scanner (Agilent Technologies). Data were extracted using Feature Extraction Software (Agilent Technologies). Data analyses were performed using Agilent Genomic Workbench 7.0 (Agilent Technologies).

Teratoma formation. 2i/L ES cells were trypsinized for single-cell suspension and 1×10^6 cells were injected subcutaneously into BALB/cSlc-nu/nu mice. At three weeks after the transplantation, formed teratomas were processed for HE staining.

Knockout using CRISPR–Cas9. sgRNA was designed using CRISPR DESIGN (http://crispr.mit.edu/). pX330-U6-Chimeric_BB-CBh-hSpCas9 was a gift from F. Zhang (Addgene plasmid no. 42230)[44]. sgRNA was ligated with px330-PGK-puro-pA. 2.5 μg of the plasmid was transfected using Xfect mES cell Transfection Reagent. Transfected cells were selected using 1 μg ml^{-1} puromycin (Sigma) for 2 days. After the selection, colonies were picked up and expanded. Each knockout 2i/L ES cells line was established after evaluation by Sanger sequencing. sgRNA sequences were: *Dnmt3a*: ACCGCCTCCTGCATGATGCG; *Dnmt3b*: AATGCACTCCTCATACCCGC; *Dnmt3l*: GCAGTATGCGCTGCCTCGCC; *Dnmt1*: CCCGTTGGCGGGACAACCGT; and *Scml2*: ATCCAGTCGTAGAC GTAACC.

***In vitro* growth assay upon induction of differentiation.** Wild type and *Dnmt*-knockout 2i/L ES cell lines were harvested into 6-well plates at a density of 5×10^4 cells per well (Day 0). To induce differentiation, PD0325901, CHIR99021 and LIF were removed from the medium, and cells were cultivated for 6 days. The number of cells was calculated at Day 2, 4 and 6 using automatic cell counter TC10 (BioRad). The experiment was performed in triplicate, and each sample was calculated twice.

Chimaera formation. Female ICR mice were treated with pregnant mare serum gonadotropin (PMSG; 7.5 IU) and human chorionic gonadotropin (hCG; 7.5 IU) by intraperitoneal (i.p.) injection. Embryos were rinsed with M2 medium (Sigma) and cultured in KSOM medium until the development into blastocysts. ES cells were trypsinized and 7–8 cells per embryo were injected into the blastocoels of E3.5 blastocysts. Injected blastocysts were transferred into the uteri of pseudo-pregnant ICR mice. Fully Automated Fluorescence Stereo Microscope Leica M205 FA (Leica MICROSYSTEMS) was used for the observation of GFP-labelled embryos.

***Cdx2*-mediated trophectoderm (TE) differentiation of ES cells.** TE differentiation of ES cells was induced by *Cdx2* overexpression as described previously[26]. Doxycycline (Dox)-inducible PB vector containing *tetO-Cdx2-IRES-mCherry-EF1-rtTA-IRES-Neo* (PB-*Cdx2*) was generated by Gateway Cloning (Invitrogen)[33]. 2.5 μg of PB-*Cdx2* and 2.5 μg of transposase were transfected using Xfect mES cell Transfection Reagent. Cells were cultured in GMEM (GIBCO) with 2 μg ml^{-1} Dox (Sigma), 350 μg ml^{-1} G418, NEAA, P/S and 10% FBS, 100 × sodium pyruvate (GIBCO), 0.11 mM β-mercaptoethanol, 2 μg ml^{-1} heparin sodium salt from porcine intestinal mucosa (Sigma), and 20 ng ml^{-1} recombinant human fibroblast growth factor 4 (Sigma) on feeders. TSC-like colonies were counted at day 7–8 after the transfection. Images for the counting were taken by BioStation CT (Nikon).

Overexpression of *Uhrf1* in female ES cells. Dox-inducible PB vector containing *tetO-Uhrf1-IRES-mCherry-EF1-rtTA-IRES-Neo* (PB-*Uhrf1*) was generated by Gateway Cloning[33]. 2.5 μg of PB-*Uhrf1* and 2.5 μg of transposase were transfected into female S/L ES cells (p4) using Xfect mES cell Transfection Reagent. Cells were cultured in medium containing 2 μg ml^{-1} Dox, and 350 μg ml^{-1} G418.

Tetraploid embryo complementation. Blastocyst injections were performed using $B_6D_2F_2$ host embryos. Female $B_6D_2F_1$ mice were treated with PMSG (7.5 IU) and hCG (7.5 IU) by i.p. injection. To obtain tetraploid (4*n*) embryos, electrofusion was performed at 42–46 h post-hCG using ECM2001 Electro Cell Manipulator (BTX). Fused embryos were cultured in KSOM until they developed blastocysts. ES cells were trypsinized and 10–12 cells per each embryo were injected into blastocoels of E3.5 4*n* blastocysts. Injected 4*n* blastocysts were transferred into the uteri of pseudo-pregnant ICR mice. Pups were recovered at E19.5 by caesarean section and fostered to lactating ICR mothers.

SSLP assay. Strain-specific primers (D1Mit303 for 129/MSM and D2Mit102 for 129/C57BL6) were used to detect the host cell's genome. The primers used were: D1Mit303 forward: GGTTTCTATTTCGGTTCTCGG; D1Mit303 reverse: TCTG

TGCTGCAAAACAGAGG; D2Mit102 forward: TTCCCTGTCACTCCTCCC; and D2Mit102 reverse: TGTCTTTATGCTCAGACATACACA. As controls, the DNA of injected ES cells and host TTFs were used.

Nuclear transfer. Mature oocytes were collected from the oviducts of $B_6D_2F_1$ female mice following PMSG and hCG by i.p. injection. Nuclear transfer was performed as described previously[23,45]. Briefly, the MII chromosome–spindle complex was aspirated into the pipette with a minimum volume of ooplasm under a droplet of H-CZB containing 5 mg ml^{-1} cytochalasin B. Each ES-cell-derived nucleus was injected into an enucleated oocyte. The reconstructed oocytes were activated using 10 mM $SrCl_2$ in Ca^{2+}-free CZB medium in the presence of 5 μM latrunculin A for 6 h[46,47]. Pseudo-pronuclear formation was examined, and the oocytes were cultured in CZB until embryo transfer at the two-cell stage. After the cloned embryos had developed to the two-cell stage the next day, they were transferred into the oviducts of pseudo-pregnant ICR strain female mice at 0.5 days post coitum (d.p.c.). At 19.5 d.p.c., the offspring were delivered by caesarean section except 10.5 d.p.c. embryo recovery.

Data availability. All data analysed by microarray, WGBS, methyl-seq and RNA-seq have been deposited in the Gene Expression Omnibus (GEO) under accession number GSE84165. GSE84165 is composed of the following two subseries, GSE82313 for microarray data and GSE84164 for DNA methylation and RNA-seq data.

31. Takada, T., Yoshiki, A., Obata, Y., Yamazaki, Y. & Shiroishi, T. NIG_MoG: a mouse genome navigator for exploring intersubspecific genetic polymorphisms. *Mamm. Genome* **26,** 331–337 (2015).
32. Tsumura, A. *et al.* Maintenance of self-renewal ability of mouse embryonic stem cells in the absence of DNA methyltransferases Dnmt1, Dnmt3a and Dnmt3b. *Genes Cells* **11,** 805–814 (2006).
33. Kim, S. I. *et al.* Inducible transgene expression in human iPS cells using versatile all-in-one *piggyBac* transposons. *Methods Mol. Biol.* **1357,** 111–131 (2016).
34. Martin, M. Cutadapt removes adapter sequences from high-throughput sequencing reads. *EMBnet.journal* **17,** 10–12 (2011).
35. Krueger, F. & Andrews, S. R. Bismark: a flexible aligner and methylation caller for Bisulfite-Seq applications. *Bioinformatics* **27,** 1571–1572 (2011).
36. Langmead, B. & Salzberg, S. L. Fast gapped-read alignment with Bowtie 2. *Nat. Methods* **9,** 357–359 (2012).
37. Robinson, J. T. *et al.* Integrative genomics viewer. *Nat. Biotechnol.* **29,** 24–26 (2011).
38. Rosenbloom, K. R. *et al.* The UCSC Genome Browser database: 2015 update. *Nucleic Acids Res.* **43,** D670–D681 (2015).
39. Illingworth, R. S. *et al.* Orphan CpG islands identify numerous conserved promoters in the mammalian genome. *PLoS Genet.* **6,** e1001134 (2010).
40. Kobayashi, H. *et al.* Contribution of intragenic DNA methylation in mouse gametic DNA methylomes to establish oocyte-specific heritable marks. *PLoS Genet.* **8,** e1002440 (2012).
41. Tomizawa, S. *et al.* Dynamic stage-specific changes in imprinted differentially methylated regions during early mammalian development and prevalence of non-CpG methylation in oocytes. *Development* **138,** 811–820 (2011).
42. Kim, D. *et al.* TopHat2: accurate alignment of transcriptomes in the presence of insertions, deletions and gene fusions. *Genome Biol.* **14,** R36 (2013).
43. Trapnell, C. *et al.* Transcript assembly and quantification by RNA-seq reveals unannotated transcripts and isoform switching during cell differentiation. *Nat. Biotechnol.* **28,** 511–515 (2010).
44. Cong, L. *et al.* Multiplex genome engineering using CRISPR/Cas systems. *Science* **339,** 819–823 (2013).
45. Wakayama, T., Rodriguez, I., Perry, A. C., Yanagimachi, R. & Mombaerts, P. Mice cloned from embryonic stem cells. *Proc. Natl Acad. Sci. USA* **96,** 14984–14989 (1999).
46. Terashita, Y. *et al.* Latrunculin A can improve the birth rate of cloned mice and simplify the nuclear transfer protocol by gently inhibiting actin polymerization. *Biol. Reprod.* **86,** 180 (2012).
47. Terashita, Y. *et al.* Latrunculin A treatment prevents abnormal chromosome segregation for successful development of cloned embryos. *PLoS One* **8,** e78380 (2013).

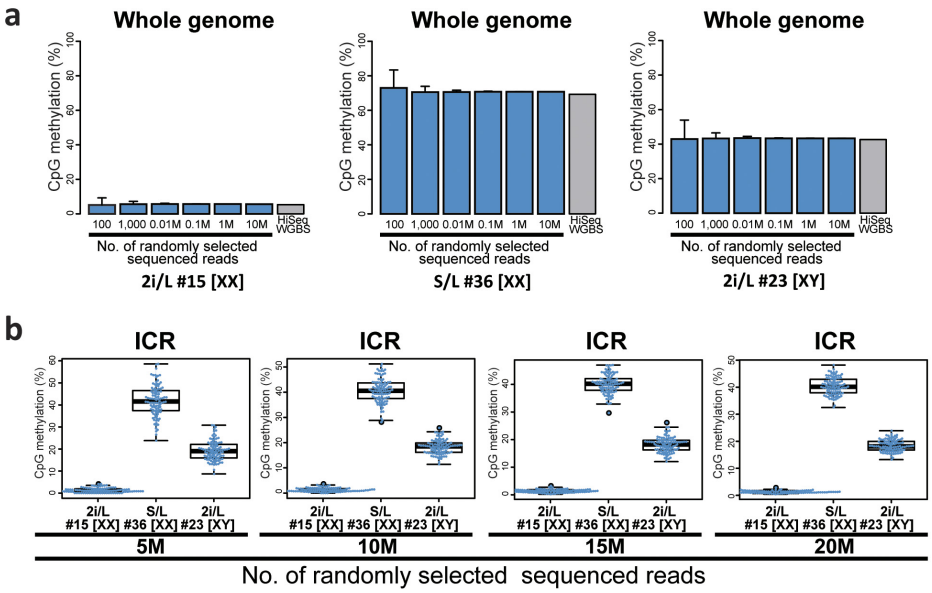

c

Cell Type	Culture Condition	Sample Name	Gender	Passage Number	Genetic Background	Method	Seq Type	Single or Pair	Read Number (Mb)	On targets (%)	Average. Depth
ES cell	2i/LIF	2i/L #2	XX	p3	129/MSM (♀/♂)	Methyl-seq	Hiseq	Pair	75.1 (×2)	89.5	64.8 (captured regions)
ES cell	2i/LIF	2i/L #15	XX	p3	129/MSM (♀/♂)	Methyl-seq	Hiseq	Pair	70.7 (×2)	89.5	59.4 (captured regions)
ES cell	2i/LIF	2i/L #23	XY	p3	129/MSM (♀/♂)	Methyl-seq	Hiseq	Pair	96 (×2)	89.3	83.1 (captured regions)
ES cell	Serum/LIF	S/L #8	XX	p3	129/MSM (♀/♂)	Methyl-seq	Hiseq	Pair	81 (×2)	88.8	67.7 (captured regions)
ES cell	Serum/LIF	S/L #36	XX	p3	129/MSM (♀/♂)	Methyl-seq	Hiseq	Pair	77.3 (×2)	89.6	66.1 (captured regions)
ES cell	Serum/LIF	2i/L-S/L #15	XX	p3+p14	129/MSM (♀/♂)	Methyl-seq	Hiseq	Pair	91.8 (×2)	89.3	78.2 (captured regions)
MEF	MEF medium	2i/L-MEFs	XX	p5+p1	129/MSM (♀/♂)	Methyl-seq	Hiseq	Pair	81.3 (×2)	88.9	68.1 (captured regions)
MEF	MEF medium	MEF#4	XX	p1	129/MSM (♀/♂)	Methyl-seq	Hiseq	Pair	90.8 (×2)	90.7	74.0 (captured regions)
MEF	MEF medium	MEF#2	XY	p1	129/MSM (♀/♂)	Methyl-seq	Hiseq	Pair	89.4 (×2)	88.5	74.2 (captured regions)
ES cell	2i/LIF	2i/L #15	XX	p3	129/MSM (♀/♂)	WGBS	Hiseq	Pair	117.3 (×2)	-	4.7
ES cell	2i/LIF	2i/L #23	XY	p3	129/MSM (♀/♂)	WGBS	Hiseq	Pair	116.9 (×2)	-	5.5
ES cell	Serum/LIF	S/L #36	XX	p3	129/MSM (♀/♂)	WGBS	Hiseq	Pair	117.6 (×2)	-	4.9
ES cell	Serum/LIF	2i/L-S/L #15	XX	p3+p14	129/MSM (♀/♂)	WGBS	Hiseq	Pair	107.9 (×2)	-	4.5

Cell Type	Culture Condition	Sample Name	Gender	Passage Number	Genetic Background	Method	Seq Type	Single or Pair	Read Number (Mb)
ES cell	2i/LIF	2i/L #15	XX	p3	129/MSM (♀/♂)	WGBS	Nextseq	Single	120.9
ES cell	2i/LIF	2i/L #23	XY	p3	129/MSM (♀/♂)	WGBS	Nextseq	Single	93.2
ES cell	Serum/LIF	S/L #36	XX	p3	129/MSM (♀/♂)	WGBS	Nextseq	Single	113.2
ES cell	2i/LIF	2i/L #2	XX	p3	129/MSM (♀/♂)	WGBS	Nextseq	Single	25.4
ES cell	2i/LIF	2i/L #20	XY	p3	129/MSM (♀/♂)	WGBS	Nextseq	Single	30.3
ES cell	Serum/LIF	S/L #8	XX	p3	129/MSM (♀/♂)	WGBS	Nextseq	Single	30
ES cell	Serum/LIF	S/L #9	XX	p3	129/MSM (♀/♂)	WGBS	Nextseq	Single	37.1
ES cell	Serum/LIF	S/L #12	XY	p3	129/MSM (♀/♂)	WGBS	Nextseq	Single	34.6
ES cell	Serum/LIF	S/L #31	XY	p3	129/MSM (♀/♂)	WGBS	Nextseq	Single	110
MEF	MEF medium	2n-2i/L-MEFs	XX	p5+p1	129/MSM (♀/♂)	WGBS	Nextseq	Single	38.5
MEF	MEF medium	4n-2i/L-MEFs	XX	p5+p1	129/MSM (♀/♂)	WGBS	Nextseq	Single	34.7
MEF	MEF medium	S/L-MEFs	XX	p5+p1	129/MSM (♀/♂)	WGBS	Nextseq	Single	27.2
ES cell	Serum/LIF	S/L #8	XX	p15	129/MSM (♀/♂)	WGBS	Nextseq	Single	33.9
ES cell	Serum/LIF	S/L #9	XX	p15	129/MSM (♀/♂)	WGBS	Nextseq	Single	32.5
ES cell	2i/LIF	2i/L #c3	XX	p3	129/B6 (♀/♂)	WGBS	Nextseq	Single	18.9
ES cell	2i/LIF	2i/L #c4	XX	p3	129/B6 (♀/♂)	WGBS	Nextseq	Single	19.9
ES cell	t2i/LIF	t2i/L #t1	XX	p3	129/B6 (♀/♂)	WGBS	Nextseq	Single	16.8
ES cell	t2i/LIF	t2i/L #t3	XX	p3	129/B6 (♀/♂)	WGBS	Nextseq	Single	19.3
ES cell	a2i/LIF	a2i/L #a4	XX	p3	129/B6 (♀/♂)	WGBS	Nextseq	Single	19.2
ES cell	a2i/LIF	a2i/L #a18	XX	p3	129/B6 (♀/♂)	WGBS	Nextseq	Single	18.7
ES cell	Serum/LIF	S/L #s17	XX	p3	129/B6 (♀/♂)	WGBS	Nextseq	Single	33.4
ES cell	Serum/LIF	S/L #s46	XX	p3	129/B6 (♀/♂)	WGBS	Nextseq	Single	38.3
ES cell	2i/LIF	2i/L #c2	XY	p3	129/B6 (♀/♂)	WGBS	Nextseq	Single	37.1
ES cell	2i/LIF	2i/L #c6	XY	p3	129/B6 (♀/♂)	WGBS	Nextseq	Single	36.1
ES cell	t2i/LIF	t2i/L #t2	XY	p3	129/B6 (♀/♂)	WGBS	Nextseq	Single	35.8
ES cell	t2i/LIF	t2i/L #t6	XY	p3	129/B6 (♀/♂)	WGBS	Nextseq	Single	32.4
ES cell	a2i/LIF	a2i/L #a1	XY	p3	129/B6 (♀/♂)	WGBS	Nextseq	Single	32.5
ES cell	a2i/LIF	a2i/L #a3	XY	p3	129/B6 (♀/♂)	WGBS	Nextseq	Single	35.5
ES cell	Serum/LIF	S/L #s10	XY	p3	129/B6 (♀/♂)	WGBS	Nextseq	Single	36.7
ES cell	Serum/LIF	S/L #s16	XY	p3	129/B6 (♀/♂)	WGBS	Nextseq	Single	31.7
ES cell	2i/LIF	2i/L #c3	XX	p15	129/B6 (♀/♂)	WGBS	Nextseq	Single	27.8
ES cell	2i/LIF	2i/L #c4	XX	p15	129/B6 (♀/♂)	WGBS	Nextseq	Single	35.7
ES cell	2i/LIF	2i/L #c2	XY	p15	129/B6 (♀/♂)	WGBS	Nextseq	Single	29.2
ES cell	2i/LIF	2i/L #c6	XY	p15	129/B6 (♀/♂)	WGBS	Nextseq	Single	26.3
ES cell	a2i/LIF	a2i/L #a4	XX	p15	129/B6 (♀/♂)	WGBS	Nextseq	Single	26
ES cell	a2i/LIF	a2i/L #a18	XX	p15	129/B6 (♀/♂)	WGBS	Nextseq	Single	24.8
ES cell	a2i/LIF	a2i/L #a1	XY	p15	129/B6 (♀/♂)	WGBS	Nextseq	Single	26.7
ES cell	a2i/LIF	a2i/L #a3	XY	p15	129/B6 (♀/♂)	WGBS	Nextseq	Single	28.1
ES cell	t2i/LIF	t2i/L #t1	XX	p15	129/B6 (♀/♂)	WGBS	Nextseq	Single	24.2
ES cell	t2i/LIF	t2i/L #t3	XX	p15	129/B6 (♀/♂)	WGBS	Nextseq	Single	19.5
ES cell	2i/LIF	2i/L #m12	XX	p1	129/B6 (♀/♂)	WGBS	Nextseq	Single	27.1
ES cell	2i/LIF	2i/L #m12	XX	p2	129/B6 (♀/♂)	WGBS	Nextseq	Single	29.9
ES cell	2i/LIF	2i/L #m12	XX	p3	129/B6 (♀/♂)	WGBS	Nextseq	Single	27.1
ES cell	2i/LIF	2i/L #m16	XX	p1	129/B6 (♀/♂)	WGBS	Nextseq	Single	23.9
ES cell	2i/LIF	2i/L #m16	XX	p2	129/B6 (♀/♂)	WGBS	Nextseq	Single	23.2
ES cell	2i/LIF	2i/L #m16	XX	p3	129/B6 (♀/♂)	WGBS	Nextseq	Single	28.6
ES cell	2i/LIF	2i/L #m22	XX	p1	129/B6 (♀/♂)	WGBS	Nextseq	Single	26.5
ES cell	2i/LIF	2i/L #m22	XX	p2	129/B6 (♀/♂)	WGBS	Nextseq	Single	28.8
ES cell	2i/LIF	2i/L #m22	XX	p3	129/B6 (♀/♂)	WGBS	Nextseq	Single	26.2

Extended Data Figure 1 | WGBS for evaluation of global and ICR methylation. The number of sequencing reads required to analyse global and ICR methylations. Sequenced reads acquired by NextSeq at single read were used for the evaluation. The indicated number of sequenced reads were randomly selected, followed by determination of global and ICR methylations. The determination was repeated 100 times. **a**, Mean ± s.d. of the 100 independent data for global DNA methylation are shown. The methylation data using sequenced reads by HighSeq (>100M reads for each sample) are shown as a control. **b**, A box-and-whisker plot of the 100 independent data for ICR methylation. Solid lines in each box indicate the median. Bottom and top of the box are lower and upper quartiles, respectively. Whiskers extend to ±1.5 interquartile range (IQR). **c**, The number of sequence reads for all samples used in this study.

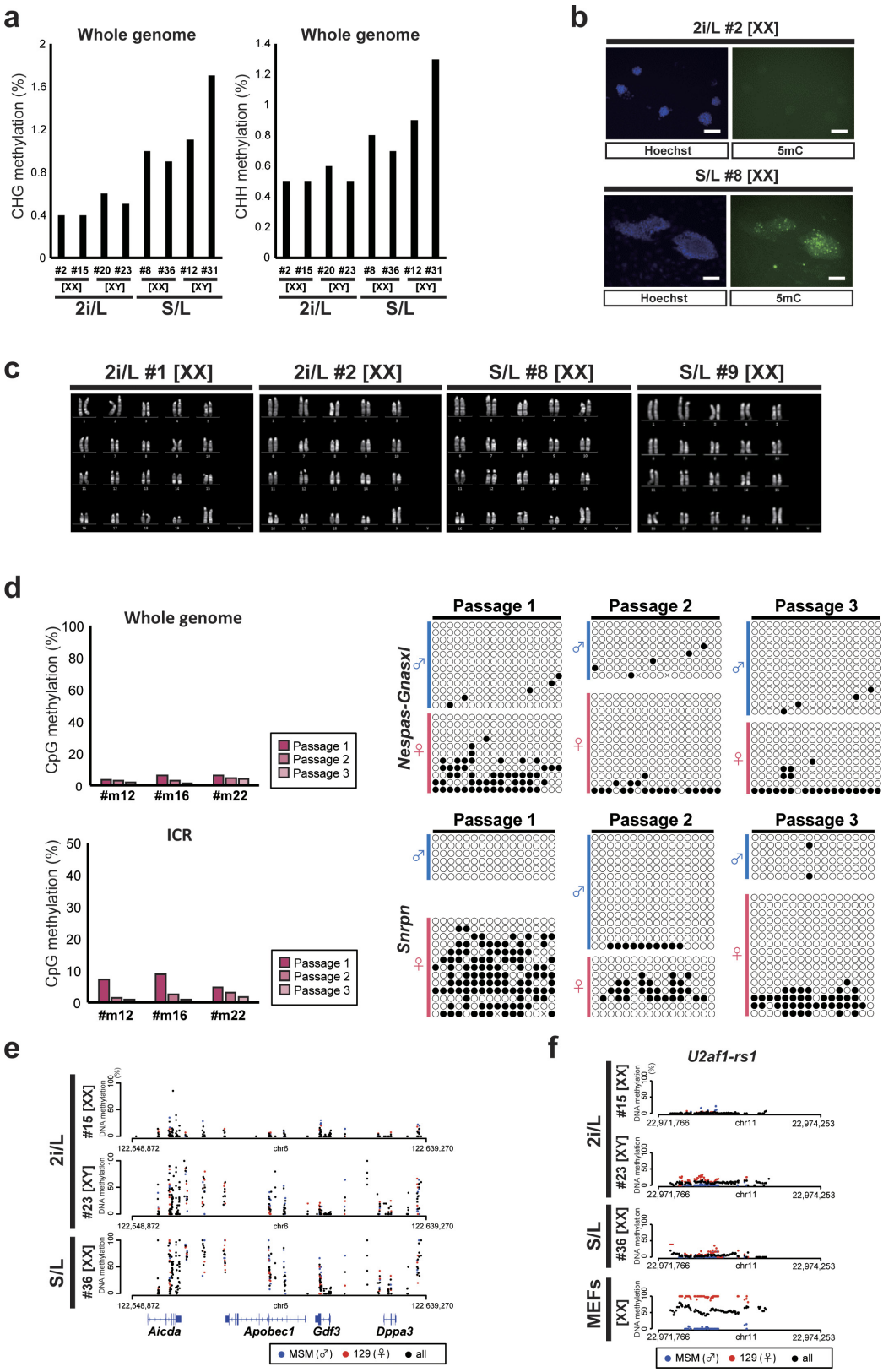

Extended Data Figure 2 | See next page for caption.

Extended Data Figure 2 | Characterization of 2i/L ES cells and S/L ES cells. a, Global CHG and CHH methylation percentages were measured by WGBS in 2i/L ES cells and S/L ES cells. DNA methylation levels are lower in 2i/L ES cells than in S/L ES cells. Two independent clones for XX and XY were analysed for 2i/L ES cells and S/L ES cells. **b**, Immunostaining for 5mC in 2i/L ES cells (#2, XX) and S/L ES cells (#8, XX). Staining signals are hardly detectable in 2i/L ES cells. Scale bars, 200 μm. **c**, Karyotype analysis by Q-band in 2i/L ES cells (#1 and #2, XX, p3) and S/L ES cells (#8 and #9, XX, p3) shows 40 chromosomes including two X chromosomes (20 cells were analysed for karyotype analysis). **d**, Dynamics of whole genome and ICR methylation levels during female 2i/L ES cell derivation (p1, p2, p3). F_1 (129/C57BL6) blastocysts were used for derivation of 2i/L ES cells. Note that a substantial reduction in both global and ICR methylation levels is already detectable at p1. The methylation levels are further reduced after passage. Independent three XX 2i/L ES cell clones were analysed. Conventional bisulfite sequencing at *Nespas-Gnasxl* and *Snrpn* ICR confirmed reduced ICR methylation at p1. Parental alleles were distinguished by SNPs (129 and C57BL6). **e**, Genome browser tracks showing representative loci that exhibit decreased methylation in 2i/L ES cells. DNA methylation in 2i/L ES cells (#15, XX, #23, XY) and S/L ES cells (#36, XX) are shown. Location of RefSeq genes and gene symbols for representative genes are indicated below. **f**, CpG methylation at *U2af1-rs1* (also known as *Zrsr1*) of 2i/L ES cells (#15, XX, #23, XY), S/L ES cells (#36, XX) and MEFs (XX). Both 2i/L ES cells and S/L ES cells revealed a substantial reduction of ICR methylation. Each black dot represents a methylation percentage for each CpG site. Red and blue dots indicate methylation levels at the maternal 129 allele and paternal MSM allele, respectively.

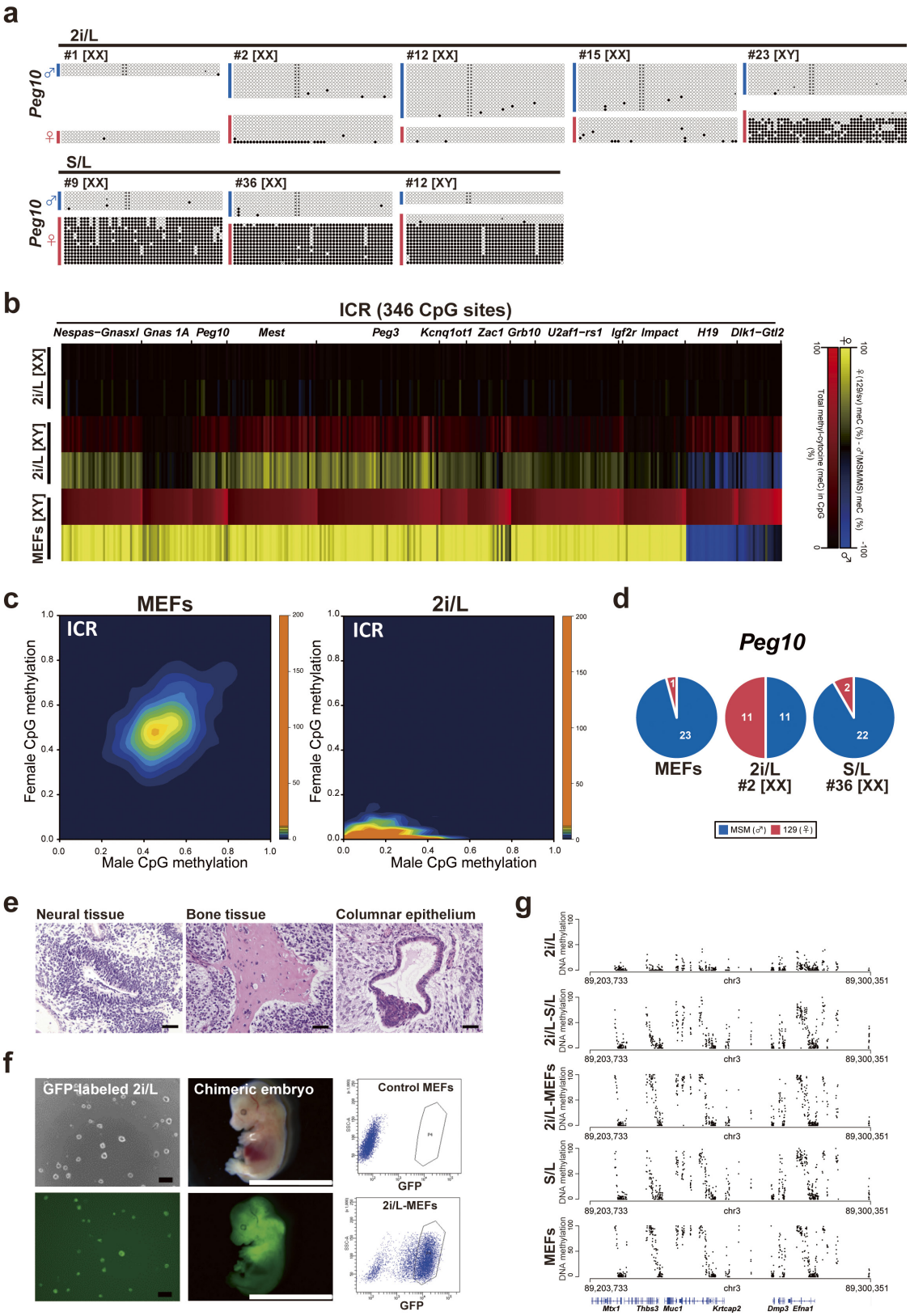

Extended Data Figure 3 | See next page for caption.

Extended Data Figure 3 | DNA methylation analyses of 2i/L ES cells, S/L ES cells and MEFs. a, Conventional bisulfite sequencing at *Peg10* DMR in multiple clones. Parental alleles were distinguished by SNPs. Open circles represent unmethylated CpGs, and closed circles represent methylated CpGs. Massive loss of CpG methylation is detected in female 2i/L ES cell lines (#1, #2, #12 and #15, XX), and erosion is observed in male 2i/L ES cells (#23, XY), whereas S/L ES cell lines (#9, #36, XX and #12, XY) often retain DMR methylation. **b**, Heat map for ICR methylation in male ES cells. ICR methylation status in 2i/L ES cells (#2, XX), 2i/L ES cells (#23, XY) and control MEFs (XY) are shown. The heat map depicts the methylation status at CpG sites in which parental alleles have been distinguished. CpG methylation levels and allelic balance for the methylation are shown for each CpG site. Both male and female 2i/L ES cells (#23, XY and #2, XX) exhibit decreased DNA methylation at ICRs. Colour scale is shown for DNA methylation levels and allelic balance. **c**, Sex differences in ICR methylation in MEFs and 2i/L ES cells. Methylation percentages of each CpG site are shown in a heat map. CpG methylation was measured by methyl-seq. Preferential reduction of ICR methylation in female cells is not observed in MEFs, while female 2i/L ES cells exhibit prominent ICR demethylation. Colour scale shows frequencies of the methylation value at each CpG site. **d**, Allelic expression analysis of the *Peg10* gene in MEFs (XY), 2i/L ES cells (#2, XX) and S/L ES cells (#36, XX). 2i/L ES cells exhibit biallelic expression of *Peg10*. Numbers of subcloned maternal/paternal alleles in RT–PCR are shown. **e**, 2i/L ES cells (#15, XX) are capable of forming teratomas, which include three different germ cell lineages (scale bars, 50 μm). **f**, GFP-labelled 2i/L ES cells (#15, XX) efficiently contributed to E14.5 embryos (scale bars of ES cells, 100 μm; scale bars of embryo, 10 mm). GFP-positive MEFs were derived from one chimaeric embryo by sorting and used for the DNA methylation analysis of 2i/L-MEFs. **g**, Genome browser tracks showing representative loci that exhibit widespread *de novo* methylation in 2i/L-S/L ES cells and 2i/L-MEFs. DNA methylation in 2i/L ES cells (#15, XX), 2i/L-S/L ES cells (#15, XX), 2i/L-MEFs (#15, XX), S/L ES cells (#36, XX) and control MEFs (XX) are shown. Location of RefSeq genes and gene symbols for representative genes are indicated below. Methyl-seq data were used for the analysis.

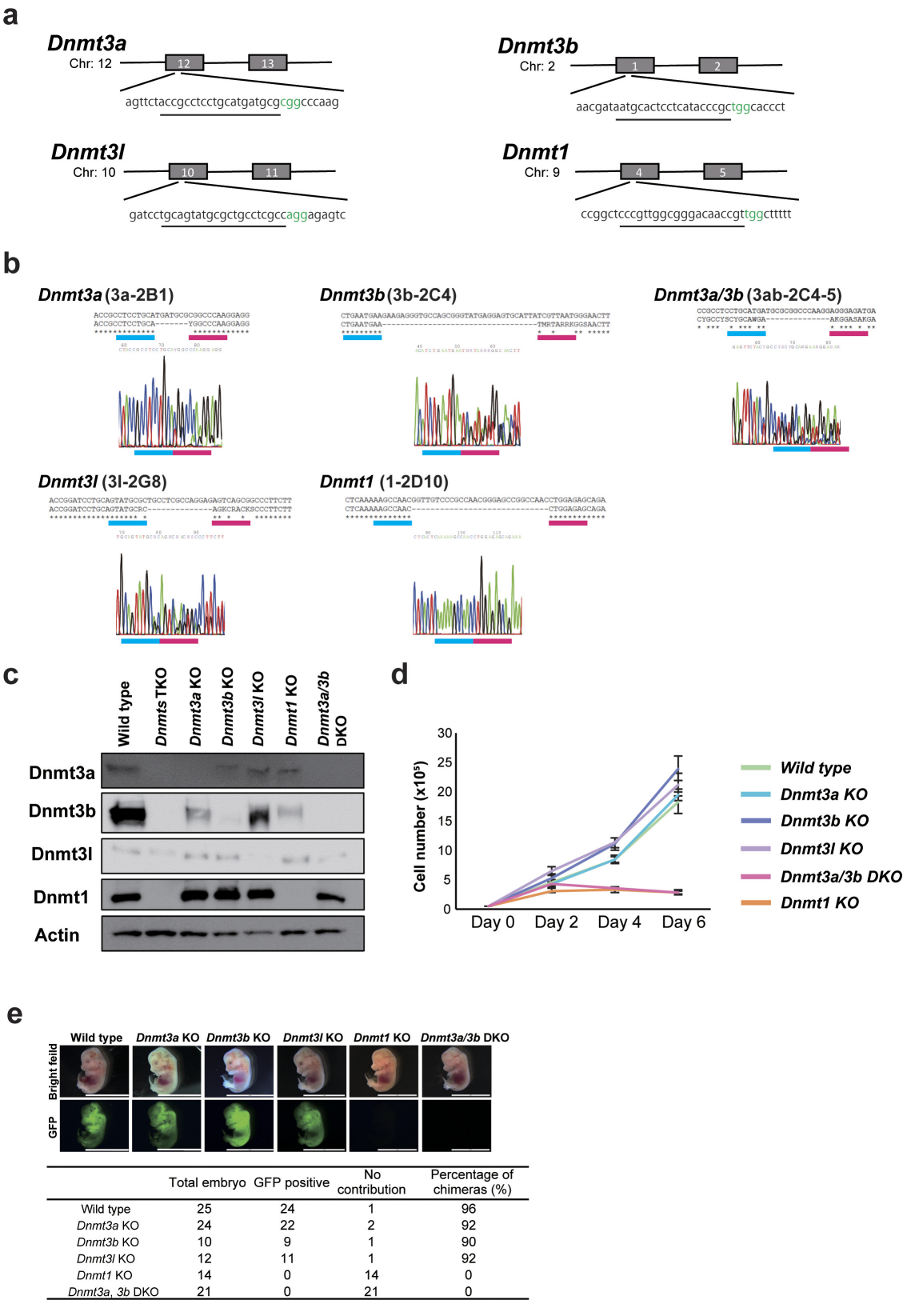

	Total embryo	GFP positive	No contribution	Percentage of chimeras (%)
Wild type	25	24	1	96
Dnmt3a KO	24	22	2	92
Dnmt3b KO	10	9	1	90
Dnmt3l KO	12	11	1	92
Dnmt1 KO	14	0	14	0
Dnmt3a, 3b DKO	21	0	21	0

Extended Data Figure 4 | See next page for caption.

Extended Data Figure 4 | Targeted disruption of *Dnmt* genes in 2i/L ES cells. a, Strategy of knockout for DNA methyltransferases using CRISPR–Cas9. Each gRNA targeting sequence is underlined, and the PAM sequence is labelled in green. 2i/L ES cells (#15, XX) were transfected with plasmids expressing CRISPR–Cas9 and gRNA in 2i/L culture condition. *Dnmt3a* was disrupted in *Dnmt3b*$^{-/-}$ ES cells to obtain double-knockout ES cells for *Dnmt3a* and *Dnmt3b*. **b**, Sanger sequencing revealed frameshift mutations in both alleles for all knockout cells. **c**, Western blotting analysis for Dnmt3a, Dnmt3b, Dnmt3l and Dnmt1 in 2i/L ES cells (wild type, #15, XX), *Dnmt* triple-knockout ES cells in serum[32], *Dnmt3a*$^{-/-}$, *Dnmt3b*$^{-/-}$, *Dnmt3l*$^{-/-}$, *Dnmt1*$^{-/-}$ and *Dnmt3a/3b*$^{-/-}$ 2i/L ES cells (#15, XX). For the detection of Dnmt3a and Dnmt3b, ES cells were cultivated in DMEM/F12 and Neurobasal supplemented with B27, N2 cell-supplements, 20 ng ml^{-1} recombinant human activin A (R&D Systems), 12 ng ml^{-1} bFGF (wako), 100 U ml^{-1} penicillin, 100 μg ml^{-1} streptomycin and 1% knockout serum replacement (GIBCO) for 2 days. **d**, Growth assay of *Dnmt*-knockout 2i/L ES cell lines cultured in the absence of 2i/L medium. Cell numbers were counted at day 0, day 2, day 4 and day 6 (independent experiments, $n = 3$). Data are presented as mean ± s.d. *Dnmt1*$^{-/-}$ and *Dnmt3a/3b*$^{-/-}$ 2i/L ES cells stopped their growth, while individual *Dnmt3*-knockout 2i/L ES cells had normal growth. **e**, Chimaeric contribution of *Dnmt*-knockout 2i/L ES cells in E14.5 embryos. For each ES cell line (p5–7), 7–8 GFP-labelled cells were injected into a 2*n* blastocyst, and 20 embryos were transferred into a pseudo-pregnant mouse. The percentage of chimaeras was calculated from the number of GFP-positive embryos out of total embryos. Scale bars, 10 mm.

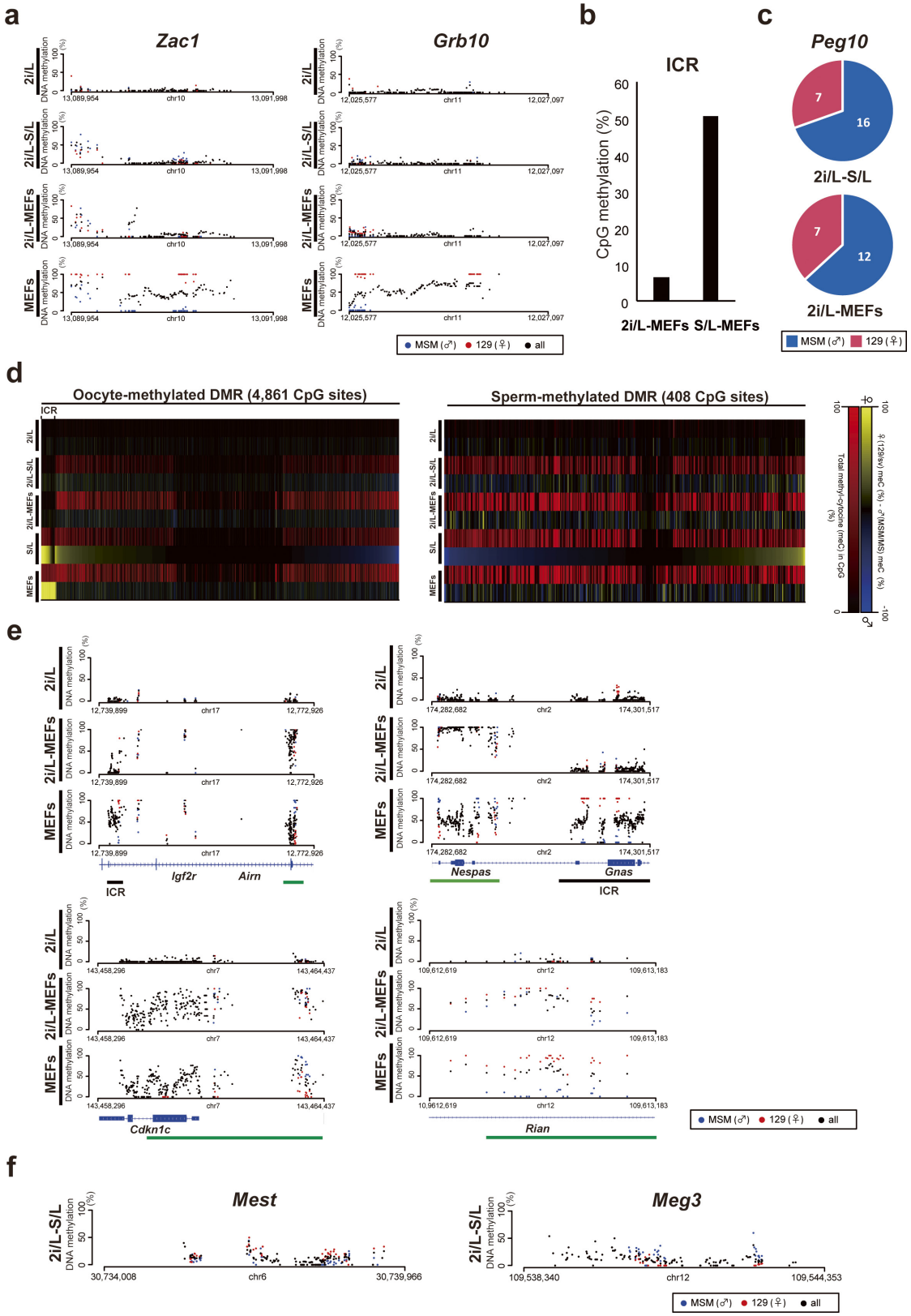

Extended Data Figure 5 | See next page for caption.

Extended Data Figure 5 | Allelic analysis of DMR methylation and gene expression. a, Individual CpG methylation levels are shown as black dots for ICRs at *Zac1* and *Grb10*. Red and blue dots indicate methylation levels at the maternal 129 allele and paternal MSM allele, respectively. Note that ICRs remain unmethylated in 2i/L-S/L ES cells (#15, XX) and 2i/L-MEFs (#15, XX). **b**, CpG methylation percentage at ICRs measured by WGBS in 2i/L-MEFs and S/L-MEFs. S/L-MEFs were derived from GFP-labelled S/L ES cells (#36, XX) at p5. Note that 2i/L-MEFs do not gain *de novo* methylation at ICRs, whereas S/L-MEFs maintain ICR methylation. **c**, Allelic expression analysis of the *Peg10* gene in 2i/L-S/L ES cells (#15, XX) and 2i/L-MEFs (#15, XX). Biallelic expression of *Peg10* is detectable in both 2i/L-S/L ES cells and 2i/L-MEFs. Numbers of subcloned maternal/paternal alleles in RT–PCR are shown. **d**, Heat map for methylation status at CpG sites in oocyte/sperm DMRs[40]. CpG methylation levels and allelic balance in 2i/L ES cells (#15, XX), 2i/L-S/L ES cells (#15, XX), 2i/L-MEFs (#15, XX), S/L ES cells (#36, XX) and control MEFs (XX) are shown. CpG sites in which parental alleles have been distinguished are included in the heat map. Most CpG sites in oocyte/sperm DMRs, except for ICRs, show *de novo* methylation. **e**, Aberrant *de novo* methylation at secondary DMR in 2i/L-MEFs. The genomic location of ICR (black) and secondary DMR (green) are shown below. **f**, Slight increase in CpG methylation is observed in a subset of ICRs. The increased methylation lacks allelic specificity.

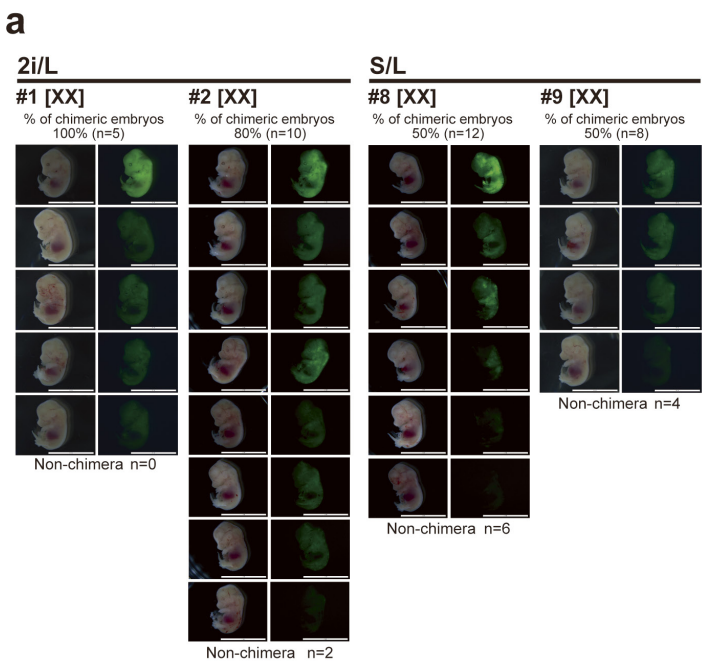

b

Cell line	No. of PN formation	2-cell	No. of ET	No. of cloned pups
2i/L #1 [XX]	134	104	104	0
2i/L #2 [XX]	148	117	117	0
S/L #8 [XX]	272	133	130	8
S/L #9 [XX]	289	145	145	3

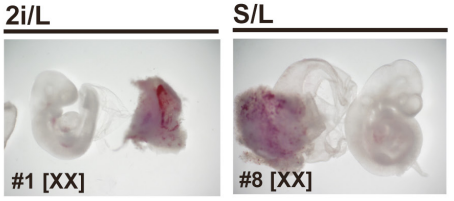

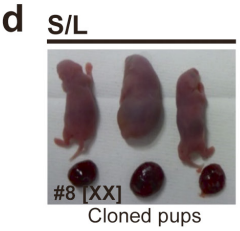

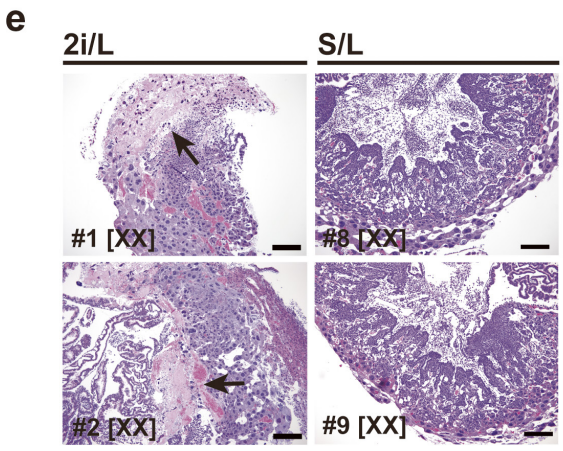

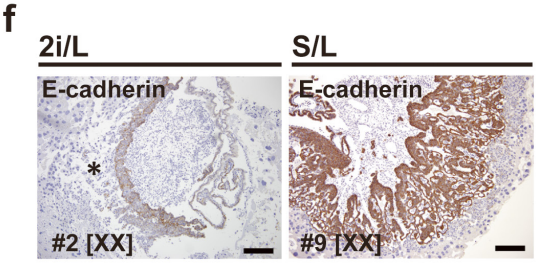

g

Cell line	No. of ET	Full term	Breathing
2i/L #1, #2 [XX]	546	0	0
S/L #8 [XX]	432	7	5

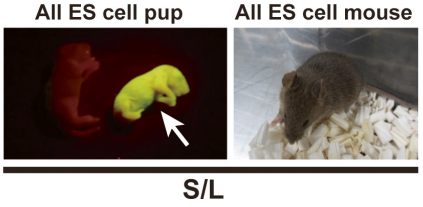

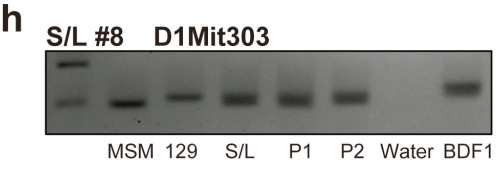

Extended Data Figure 6 | See next page for caption.

Extended Data Figure 6 | Comparison of developmental potential of 2i/L ES cells and S/L ES cells. a, Efficient contribution of 2i/L ES cells to E14.5 chimaeric embryos. GFP-labelled 2i/L ES cells (#1, XX and #2, XX, p5–6) and S/L ES cells (#8, XX and #9, XX, p5–6) were injected into diploid blastocysts, and the injected embryos were transplanted into the uteri of pseudo-pregnant mice. The number of obtained embryos for 2i/L ES cells #1, 2i/L ES cells #2, S/L ES cells #8 and S/L ES cells #9 is 5, 10, 12 and 8, respectively. Scale bars, 10 mm. **b**, Table shows results of nuclear transfer, including the number of cells that formed pronuclei (PN), developed into 2-cell-stage embryos, used for embryo transfer (ET) and produced cloned pups. **c**, E10.5 cloned embryo from 2i/L ES cell nucleus shows growth retardation phenotype. **d**, Representative image of cloned pups derived from S/L ES cells. Cloned pups were obtained only from S/L ES cells (#8, XX and #9, XX). **e**, Histological analysis of the cloned placentae (E10.5). Representative histological images of the cloned placentae are shown. Scale bars, 500 μm. Hypoplasia of the labyrinth layer and focal necrosis (arrows) were detectable in the placentae from 2i/L ES cell nuclei. Number of cloned placentae examined: 2i/L ES cells #1; $n = 8$, 2i/L ES cells #2; $n = 11$, S/L ES cells #8; $n = 7$, and S/L ES cells #9; $n = 9$. **f**, Immunostaining reveals the reduced expression of E-cadherin in 2i/L-ES-cell-cloned placentae. Hypoplasia of the labyrinth layer and impaired cell adhesion are shown by the asterisk. Number of cloned placentae examined: 2i/L ES cells #1; $n = 8$, 2i/L ES cells #2; $n = 11$, S/L ES cells #8; $n = 7$, and S/L ES cells #9; $n = 9$. **g**, *4n* complementation results of 2i/L ES cells and S/L ES cells showing numbers of embryos transferred, full-term pups, and breathing. Images show a GFP-positive all-ES-cell pup (arrow) and an all-ES-cell mouse at 3 weeks of age (right). **h**, Confirmation of the origin of all-ES-cell pups (pup1 and pup2) by simple sequence length polymorphism (SSLP) using genomic DNA isolated from the original S/L ES cells (#8, XX), pup1, and pup2 in comparison with MSM/Ms and 129X1/SvJ genomic DNA. Genomic DNA from BDF1 mouse was used as control for host blastocyst-derived cells.

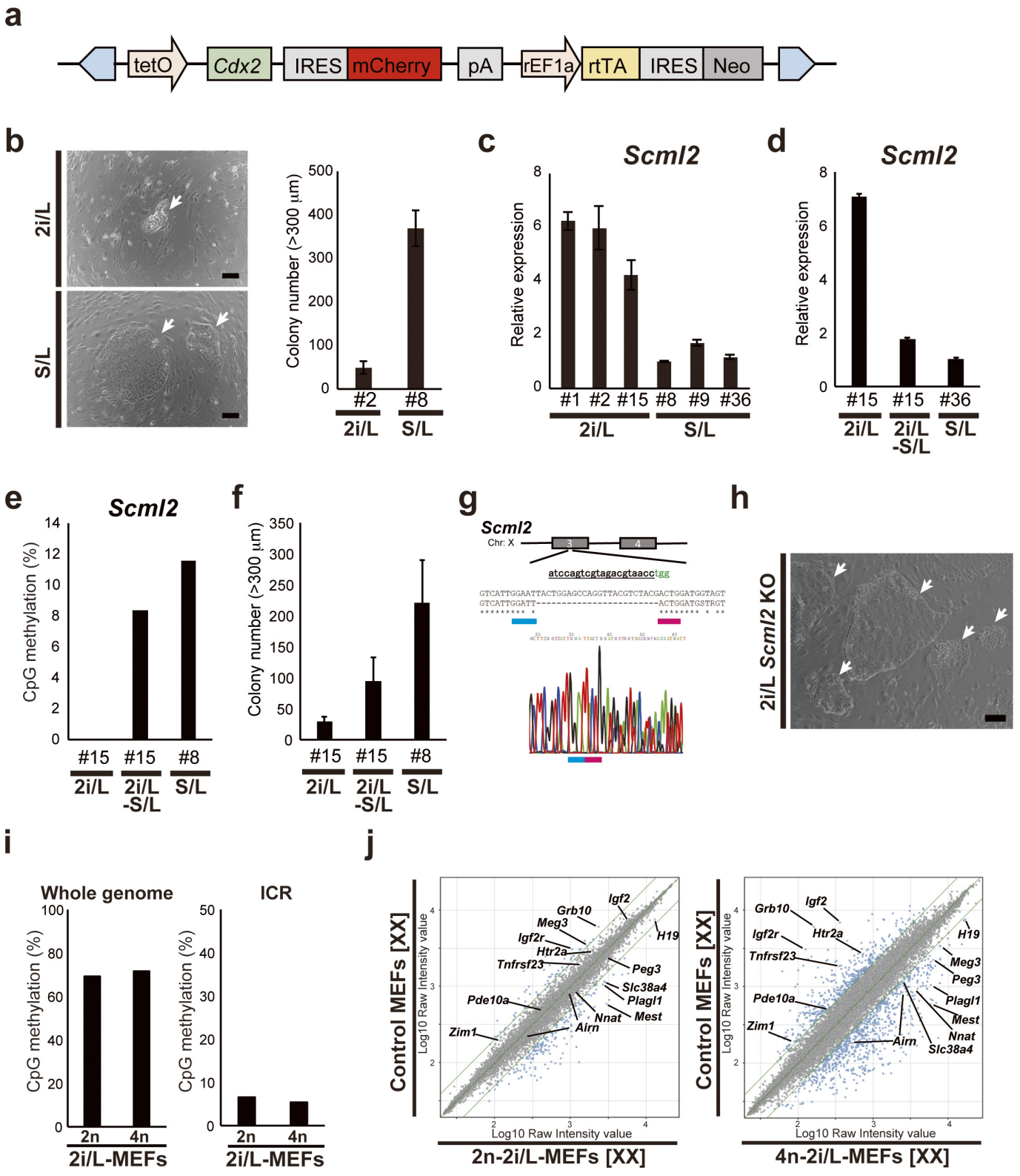

Extended Data Figure 7 | See next page for caption.

Extended Data Figure 7 | Loss of gamete-derived methylation is associated with impaired developmental potential of 2i/L ES cells. **a**, Doxycycline (Dox)-inducible *piggyBac* vector containing *tetO-Cdx2-IRES-mCherry-EF1-rtTA-IRES-Neo* (PB-*Cdx2*). **b**, Mean ± s.d. of trophoblast stem cell (TSC)-like colony number after ectopic *Cdx2* expression in ES cells. Impaired colony formation was observed in 2i/L ES cells. The number of TSC-like colonies (>300 μm) per 6-well plate is shown (independent experiments, $n = 3$). **c**, qRT–PCR analysis for *Scml2* in 2i/L ES cells and S/L ES cells. 2i/L ES cells exhibit an increased expression of *Scml2*. Data are presented as the mean ± s.d. The mean expression level of S/L ES cells (#8) was set to 1 (technical replicates, $n = 3$). **d**, qRT–PCR analysis for *Scml2* in 2i/L ES cells, 2i/L-S/L ES cells and S/L ES cells. *Scml2* expression was repressed in 2i/L-S/L ES cells compared to 2i/L ES cells. Data are presented as the mean ± s.d. The mean expression level of S/L ES cells (#36) was set to 1 (technical replicates, $n = 3$). **e**, Maternal *Scml2* methylation in 2i/L ES cells (#15, XX), 2i/L-S/L ES cells (#15, XX) and S/L ES cells (#8, XX). CpG sites in which maternal allele has been distinguished were used to determine DNA methylation levels at *Scml2* (TSS ± 1,000 bp). Methyl-seq data were used for the analysis. **f**, Impaired capacity of TSC-like colony formation was partially rescued by serum exposure. Data are mean ± s.d. (independent experiments, $n = 3$). **g**, Strategy of knockout for *Scml2* using CRISPR–Cas9. gRNA targeting sequence is underlined, and the PAM sequence is labelled in green. 2i/L ES cells (#2, XX) were transfected with plasmids expressing CRISPR–Cas9 and gRNA in 2i/L culture condition. **h**, Genetic disruption of *Scml2* partially rescued the impaired colony formation in 2i/L ES cells. **i**, DNA methylation analysis for 2i/L-MEFs. 4*n* 2i/L-MEFs and 2*n* 2i/L-MEFs (E14.5) exhibit similar methylation levels. ICR methylation data of 2*n* 2i/L-MEFs is the same as Extended Data Fig. 5b. **j**, Microarray analysis shows aberrant global gene expression in 4*n* 2i/L-MEFs. Note that the most affected genes often include imprinted genes. Green lines are fold change lines with a value of 2.0. Representative imprinted genes with altered expression are indicated in the scatter plot.

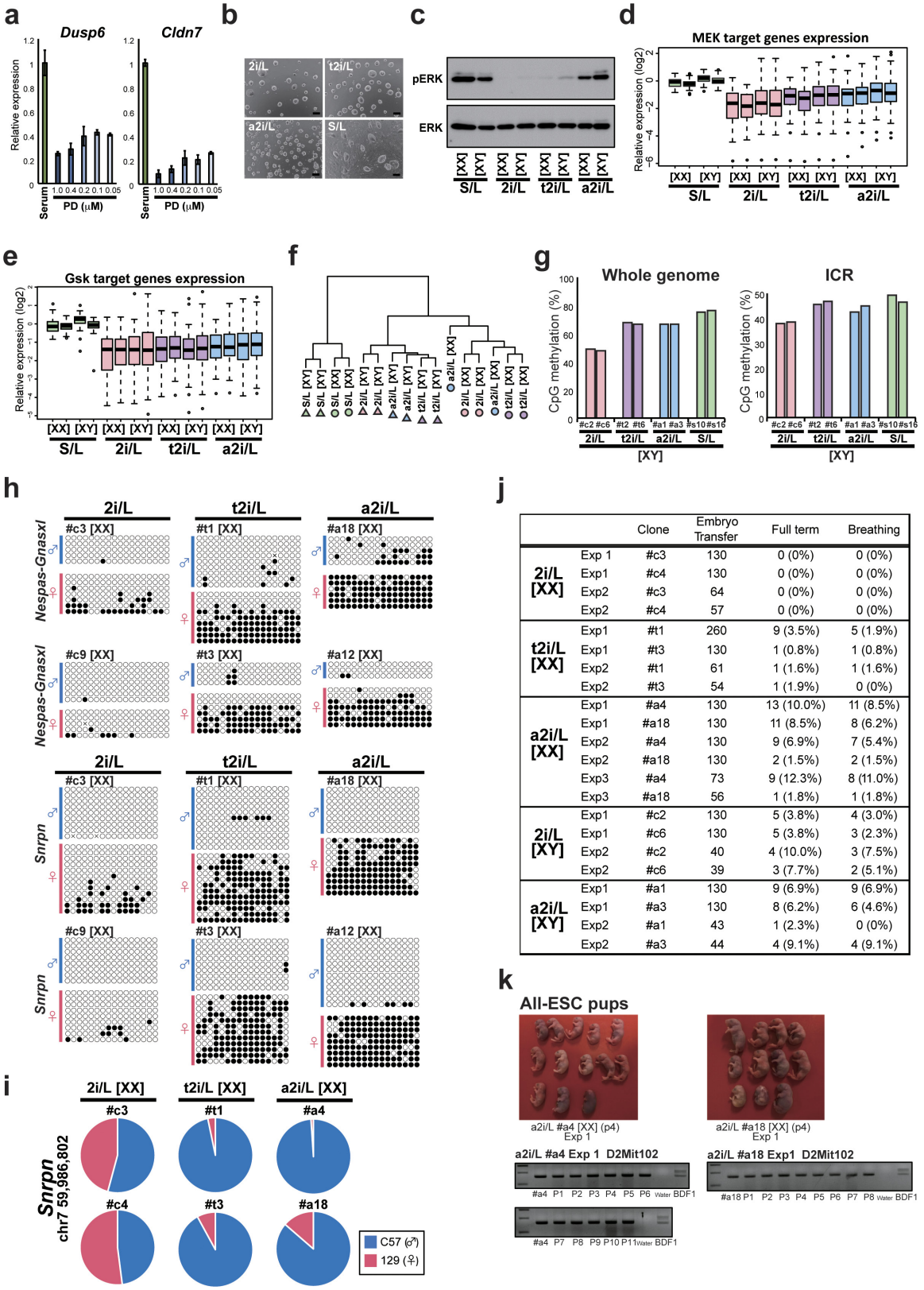

		Clone	Embryo Transfer	Full term	Breathing
2i/L [XX]	Exp 1	#c3	130	0 (0%)	0 (0%)
	Exp1	#c4	130	0 (0%)	0 (0%)
	Exp2	#c3	64	0 (0%)	0 (0%)
	Exp2	#c4	57	0 (0%)	0 (0%)
t2i/L [XX]	Exp1	#t1	260	9 (3.5%)	5 (1.9%)
	Exp1	#t3	130	1 (0.8%)	1 (0.8%)
	Exp2	#t1	61	1 (1.6%)	1 (1.6%)
	Exp2	#t3	54	1 (1.9%)	0 (0%)
a2i/L [XX]	Exp1	#a4	130	13 (10.0%)	11 (8.5%)
	Exp1	#a18	130	11 (8.5%)	8 (6.2%)
	Exp2	#a4	130	9 (6.9%)	7 (5.4%)
	Exp2	#a18	130	2 (1.5%)	2 (1.5%)
	Exp3	#a4	73	9 (12.3%)	8 (11.0%)
	Exp3	#a18	56	1 (1.8%)	1 (1.8%)
2i/L [XY]	Exp1	#c2	130	5 (3.8%)	4 (3.0%)
	Exp1	#c6	130	5 (3.8%)	3 (2.3%)
	Exp2	#c2	40	4 (10.0%)	3 (7.5%)
	Exp2	#c6	39	3 (7.7%)	2 (5.1%)
a2i/L [XY]	Exp1	#a1	130	9 (6.9%)	9 (6.9%)
	Exp1	#a3	130	8 (6.2%)	6 (4.6%)
	Exp2	#a1	43	1 (2.3%)	0 (0%)
	Exp2	#a3	44	4 (9.1%)	4 (9.1%)

Extended Data Figure 8 | See next page for caption.

Extended Data Figure 8 | Derivation of ground-state ES cells maintaining ICR methylation. a, A qRT–PCR analysis for representative Mek target genes (*Dusp6* and *Cldn7*) in ES cells under various PD concentrations and 3μM CHIR. Attenuated repression of these genes was observed until the concentration decreased to 0.2 μM. Data are presented as the mean ± s.d. The mean expression level of S/L ES cells was set to 1 (technical replicates, $n = 3$). **b**, Representative morphology of ES cells under various culture conditions. Scale bars, 100 μm. **c**, Effect of ES-cell-derivation conditions on phosphorylation of ERK1/2 by western blot. **d**, The relative expressions of Mek target genes in ES cells[27]. The mean expression level of S/L ES cell lines was set to 1. Two independent clones at p3 were analysed for each culture condition. **e**, The relative expressions of Gsk target genes in ES cells[27] established under various culture conditions. The repression of Gsk target genes is similarly observed in 2i/L, t2i/L and a2i/L ES cells. Two independent clones at p3 were analysed for each culture condition. The mean expression level at S/L ES cell lines was set to 1. **f**, Hierarchical clustering analysis by RNA-seq data depicts t2i/L ES cells and a2i/L ES cells as having similar expression signatures with 2i/L ES cells (independent ES cell clones; $n = 2$ for each condition and sex). All expressed genes including X-linked genes were used for this analysis. **g**, DNA methylation percentage of the whole genome and ICR measured by WGBS in male ES cell lines established under various culture conditions. **h**, Conventional bisulfite sequencing at *Nespas-Gnasxl* and *Snrpn* ICR in multiple clones. Parental alleles were distinguished by SNPs (129 and C57BL6). Note that t2i/L ES cells and a2i/L ES cells tend to retain ICR methylation at maternal allele. **i**, Allelic expression analysis of *Snrpn* gene in female 2i/L ES cells, t2i/L ES cells and a2i/L ES cells. RNA-seq analysis reveals that *Snrpn* tends to be expressed monoallelically in t2i/L ES cells and a2i/L ES cells, whereas the biallelic expression is observed in 2i/L ES cells. **j**, Efficiency of 4*n* complementation using 2i/L, t2i/L and a2i/L ES cells. **k**, Images show all-ES-cell pups originated from female a2i/L ES cells. The origin of all-ES-cell pups was confirmed by SSLP. Genomic DNA from the BDF1 mouse was used as a control for host blastocyst-derived cells.

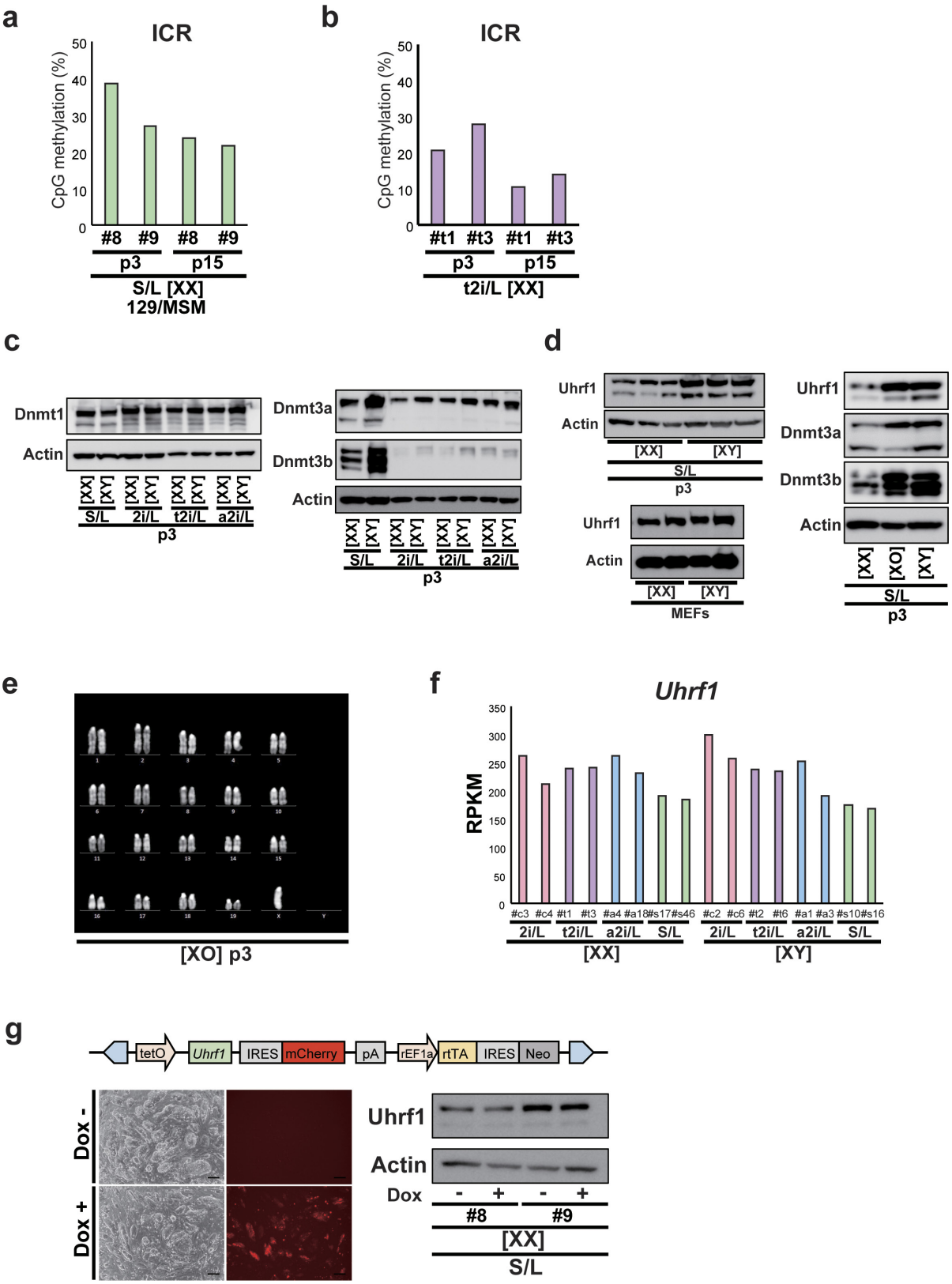

Extended Data Figure 9 | See next page for caption.

Extended Data Figure 9 | Decreased levels of Uhrf1 protein in female ES cells. a, Reduction of ICR methylation in female S/L ES cells after prolonged culture. Methylation data of S/L ES cells #8 at p3 are the same as Fig. 1d. **b**, ICR methylation level in female t2i/L ES cells at p3 and p15. Methylation data of t2i/L ES cells #t1 and #t3 at p3 are the same as Fig. 4d. **c**, Western blotting of DNA methyltransferases. Dnmt3a and Dnmt3b levels are lower in female ES cells. Dnmt3b was strongly repressed in 2i/L, t2i/L and a2i/L culture conditions. The Dnmt1 level is comparable between male and female ES cells. **d**, Western blotting for Uhrf1 in multiple S/L ES cells and MEFs and for Uhrf1, Dnmt3a and Dnmt3b in XX/XO/XY S/L ES cells. Note that Uhrf1 protein levels are decreased in female ES cells but not in female MEFs and XO ES cells, suggesting that two active X chromosomes are associated with the decreased Uhrf1 protein level. **e**, Karyotype analysis by Q-band in S/L ES cells (#s100, p3) unexpectedly revealed 39 chromosomes containing a single X chromosome but lacking a Y chromosome. Of 20 cells, 15 exhibited loss of the Y chromosome. **f**, Transcript levels of *Uhrf1* in ES cells by RNA-seq. *Uhrf1* is similarly expressed in both male and female ES cells regardless of culture conditions. **g**, Ectopic expression of *Uhrf1* by Dox-inducible *piggyBac* vector in female S/L ES cells. mCherry signal confirmed successful induction of the transgene. Scale bars, 100 μm. Uhrf1 protein is not increased in female ES cells by Dox treatment (2 μg ml^{-1}).

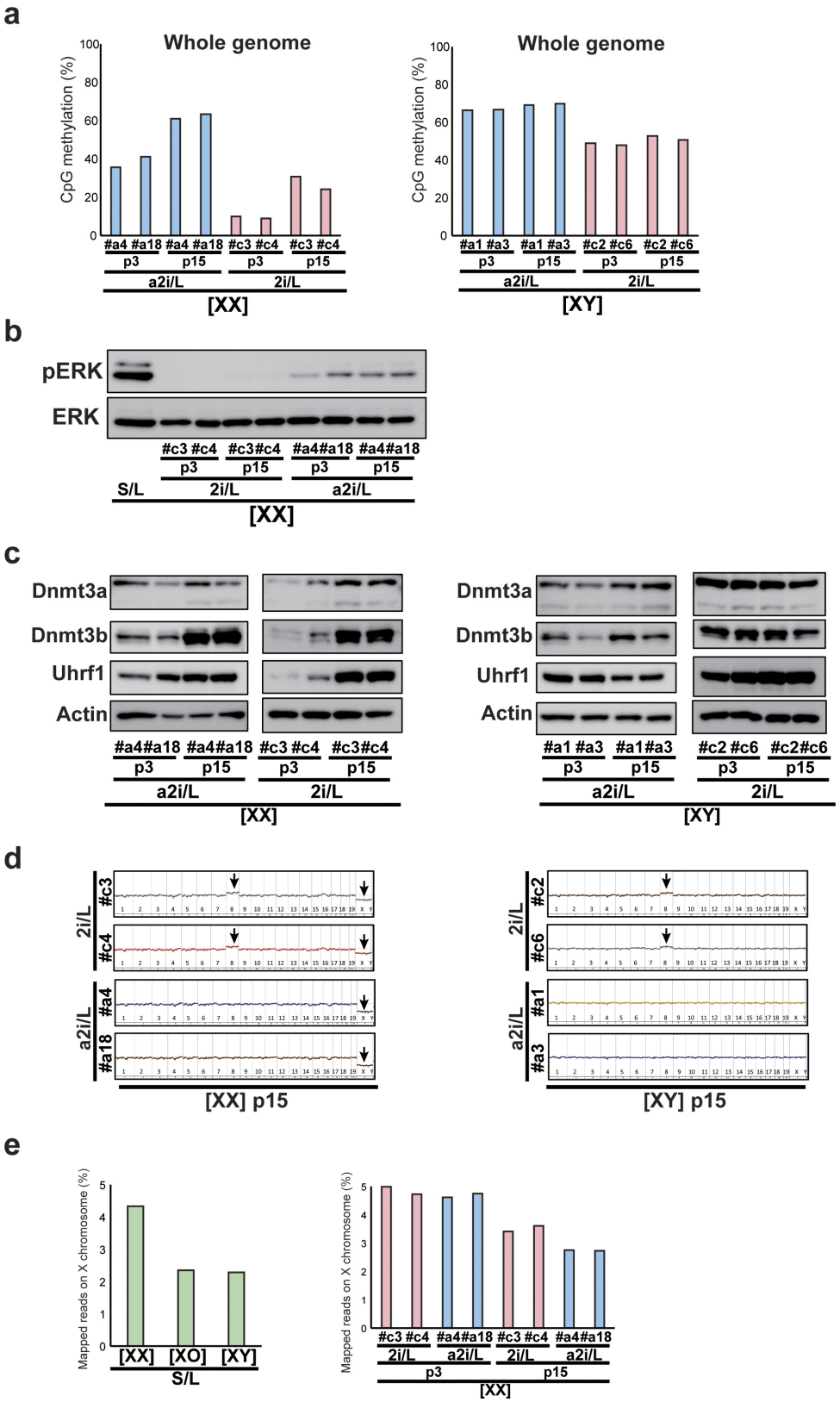

Extended Data Figure 10 | See next page for caption.

Extended Data Figure 10 | Increased global DNA methylation and loss of X chromosome in female 2i/L and a2i/L ES cells after prolonged culture. a, Effect of prolonged culture on global DNA methylation in 2i/L and a2i/L ES cells. Global DNA methylation is increased in female 2i/L and a2i/L ES cells after prolonged culture (p15). Methylation data of female a2i/L ES cells (#a4, #a18) at p3, female 2i/L ES cells (#c3, #c4) at p3, male a2i/L ES cells (#a1, #a3) at p3 and male 2i/L ES cells (#c2, #c6) at p3 were the same as Fig. 4d and Extended Data Fig. 8g. **b**, pERK of female 2i/L and a2i/L ES cells at p15 are similarly repressed compared with their identical clones at p3. **c**, Prolonged passage results in an increment of Dnmt3b and Uhrf1 protein levels in female 2i/L and a2i/L ES cells but not in male ES cells. **d**, CGH analysis depicting partial loss of the X chromosome in female 2i/L and a2i/L ES cells after prolonged culture (p15). Gain of chromosome 8 is observed in both male and female 2i/L ES cells, but not in a2i/L ES cells. **e**, Mapping efficiency of WGBS reads on the X chromosome in early passage (p3) and late passage (p15) female 2i/L and a2i/L ES cells (#c3, XX; #c4, XX; #a4, XX; #a18, XX). Consistent with the loss of the X chromosome in the CGH analysis, decreased mapping of WGBS reads on the X chromosome is observed in female 2i/L and a2i/L ES cells at p15. Note that the identical ES cell lines at p3 do not display decreased mapping efficiency on the X chromosome, indicating that the female 2i/L and a2i/L ES cell lines have lost the X chromosome during prolonged culture. XX, XO, XY S/L ES cells are shown as controls of X chromosome mapping.